ELSEVIER

Tectonophysics 341 (2001) 69–93

TECTONOPHYSICS

www.elsevier.com/locate/tecto

Bulk flow strength of forsterite–enstatite composites as a function of forsterite content

Shaocheng Ji [a,*], Zichao Wang [a], Richard Wirth [b]

[a] *Département des Génies Civil, Géologique et des Mines, École Polytechnique de Montréal, C.P. 6709, Succursale Centre-Ville, Montréal, Québec, Canada H3C 1J4*

[b] *GFZ-Potsdam, Telegrafenberg, D-14473, Potsdam, Germany*

Received 20 January 2000; accepted 28 August 2001

Abstract

Creep experiments have been conducted to investigate the effect of varying forsterite content (V_{Fo}) on the bulk flow strength of dry forsterite–enstatite (Fo–En) aggregates in order to evaluate the applicability of existing theoretical models to two-phase rocks, as well as to understand the rheology of polyphase systems in general. The experiments were performed at temperatures of 1423–1593 K, stresses of 18–100 MPa, oxygen fugacities of 10^{-14}–$10^{-2.5}$ MPa and 0.1 MPa total pressure. The fine-grained (Fo: 10–17 μm; En: 14–31 μm) composites of various Fo volume fractions (V_{Fo} = 0, 0.2, 0.4, 0.5, 0.6, 0.8 and 1) were synthesized by isostatically hot-pressing in a gas-medium apparatus at 1523 and 350 MPa. Our experiments show that flow strength contrasts between Fo and En are in the range of 3–8 at the given experimental conditions, with Fo as the stronger phase. The measured stress exponent (n) and activation energy (Q) values of the Fo–En composites fall between those of the end-members. The n values show a nearly linear increase from 1.3 to 2.0, while the Q values display a non-linear increase from 472 to 584 kJ/mol with En volume fraction from 0 to 1.0. There is no clear dependence of creep rates on oxygen fugacity for the Fo–En composites. The mechanical data and TEM microstructural observations suggest no change in deformation mechanism of each phase when in the composites, compared to when in a single-phase aggregate, the En deformed mainly by dislocation creep while the Fo deformed by dislocation-accommodated diffusion creep for our grain sizes and experimental conditions. Comparisons between the measured composite strengths and various theoretical models indicate that none of the existing theoretical models can give a precise predication over the entire V_{Fo} range from 0 to 1. However, the theoretical models based on weak-phase supported structures (WPS) yield a good prediction for the flow strengths of the composites with $V_{Fo} < 0.4$, while those based on strong-phase supported structures (SPS) are better for the composites with $V_{Fo} > 0.6$. No model gives a good prediction for the bulk strength of two-phase composites in the transitional regime ($V_{Fo} = 0.4$–0.6). Applications of the WPS- and SPS-based models in the transitional regime result in under- and over-estimations for the composite flow strength, respectively. Thus, the effect of rock microstructure should be taken into consideration in modeling the bulk flow strengths of the crust and upper mantle using laboratory-determined flow laws of single-phase aggregates. © 2001 Elsevier Science B.V. All rights reserved.

Keywords: Forsterite–enstatite composites; Flow strength; Plasticity; Rheology; Upper mantle

* Corresponding author. Fax: +1-514-3403970.
E-mail address: sji@courriel.polymtl.ca (S. Ji).

0040-1951/01/$ - see front matter © 2001 Elsevier Science B.V. All rights reserved.
PII: S0040-1951(01)00191-3

1. Introduction

The continuity and interconnectivity of constitutive minerals play an important role in the rheological behavior of rocks (Burg and Wilson, 1987; Jordan, 1988; Handy, 1994). The drastic decrease in bulk flow strength with a transition from strong-phase supported structure (SPS) to weak-phase supported structure (WPS) is considered to be critical phenomenon in the rheology of two-phase rocks (Arzi, 1978; Gilotti, 1992; Rutter and Neumann, 1995). What is the critical weak-phase fraction at which such a transition takes place in a solid two-phase composite? To what extent does the flow strength drop after the critical weak-phase fraction has reached? Does deformation mechanism of each phase change when in the composite as compared to when it is in a single-phase aggregate? If there is no change in deformation mechanism of each phase due to the phase mixing, how precisely can we predict variations of the flow properties of two-phase composites as a function of the volume fractions, phase continuities and flow laws of the end-members using existent theoretical models? In this study, high-temperature creep experiments were performed on forsterite–enstatite (Fo–En) composites and the experimental results were carefully compared with the theoretical models, in an attempt to answer the above questions.

Three main factors lead us to choose the olivine–orthopyroxene system as a model composite. First, olivine and orthopyroxene are two major mineral phases stable in the Earth's upper mantle above the transition zone. To a first approximation, the rheology of the upper mantle can be represented by that of olivine–orthopyroxene composites. The knowledge of the rheological properties of the upper mantle is important for understanding a wide range of tectonic processes, such as convection of the upper mantle and subduction of lithospheric slabs. Second, the high temperature plasticity of both olivine and orthopyroxene have been extensively studied by many researchers (see Darot and Gueguen, 1981; Relandeau, 1981; Karato et al., 1986; Bai et al., 1991; Kohlstedt et al., 1995 for a review). Accurate knowledge of the plasticity of the end-members is necessary for testing the relevance of the mixture rules used for the prediction of composite flow strength. Third, Hitchings et al. (1989) reported that olivine–orthopyroxene aggregates are weaker than the end-members, although Daines and Kohlstedt (1996) and McDonnell et al. (2000) found that no significant difference in flow strength between olivine–orthopyroxene aggregates with orthopyroxene contents up to 20 vol.%. Bruhn et al. (1999) documented a significant rheological weakening for calcite–anhydrite (50:50) composites compared to end-member flow strengths. Such a rheological weakening for a two-phase mixture violates most of the mixing rules in the literature of material sciences assuming no change in deformation mechanism of each phase when in the composites as compared to when a single-phase aggregate. Bruhn et al. (1999) attributed the observed weakening to operation of deformation mechanisms in the mixture that are not operative in the end-member aggregates (e.g., more rapid diffusion along phase boundaries than along grain boundaries). A systematic investigation is thus needed to verify if such behavior occurs in composites other than calcite–anhydrite one.

2. Experimental technique and procedure

2.1. Forsterite–enstatite composite samples

Forsterite (Mg_2SiO_4) is stable up to its melting temperature ($T_m = \sim 2173$ K) at 0.1 MPa pressure. Enstatite ($MgSiO_3$) may undergo several structural phase transformations with temperature (T) and pressure (P). At $P = 0.1$ MPa, the enstatite has a protoenstatite structure at high T (>1273 K) and an orthoenstatite structure at low T (923–1273 K) (Anastasiou and Seifert, 1972). The orthoenstatite may revert to clinoenstatite upon quenching to ambient conditions. The Fo–En composite samples used in this study were prepared through a two-stage sintering–hot pressing technique. No water was added into the samples during either stage of the hot pressing. We first synthesized Fo and En separately in a box furnace at temperatures close to $0.8–0.9T_m$ of the En ($T_m = \sim 1813$ K) and Fo, respectively, using chemical compounds MgO and SiO_2 as starting materials. Sintered products were examined by using X-ray powder diffraction. The Fo was identified by well-established diffraction peaks, but the diffraction pattern of En was complicated with peaks for both clinoenstatite and protoenstatite. The

clinoenstatite may have formed during cooling. We assume that the protoenstatite is the dominant phase during high temperature deformation based on the phase diagram of Presnall (1995).

Synthetic Fo and En powders were crushed, ground in an agate mill, and sieved to produce fine-grained powders with grain sizes smaller than 60 μm. Fine-grained (< 10 μm) powders, which were used as starting material for producing Fo–En composites, were obtained by settling in distilled water. The Fo and En powders were then mixed mechanically, with forsterite volume fractions (V_{Fo}) of 0 (Fo0), 0.2 (Fo20), 0.4 (Fo40), 0.5 (Fo50), 0.6 (Fo60), 0.8 (Fo80), and 1.0 (Fo100, first in ethanol for 24–30 h and then in a motor-driven agate mill for about 48 h. The mixed two-phase powder was dried for at least 72 h at 423 K before being cold-pressed into Ni cans (25 mm in length, 15 mm in diameter). The cold-pressed samples were finally isostatic ally hot-pressed at 1523 K and 350 MPa for 5 h in an internally heated gas-medium apparatus using argon as the confining medium (GFZ-Potsdam, Germany). During the hot-pressing, the oxygen was buffered at Ni–NiO by oxidation of the Ni can.

After hot-pressing, the composite samples were examined with optical microscopy, scanning electron microscopy (SEM), transmission electron microscopy (TEM) and powder X-ray diffraction. The synthetic composite samples, in general, showed a granular texture with quasi-equilibrium grain boundaries (Fig. 1a–b). Both Fo and En phases are homogeneously distributed. We did not observe clusters of either En or Fo phase at optical scale. TEM observations showed neither melt pockets in triple junctions nor melt films along the Fo/En, Fo/Fo or En/En grain boundaries. The boundaries are straight and clean (Fig. 1b). Most of the Fo/Fo and En/En grain boundaries are coherent and high-angle, suggesting that the synthesis and compaction of samples were well done. The En grains often contain growth twins (Fig. 1b), which are believed to form during the quenching. Scattered distributed dislocation loops or short free dislocations can be seen in both Fo and En grains (Fig. 1b), but the average dislocation density is very low ($< 2 \times 10^{12}$ m^{-2}).

Sample densities were measured using Archimedes' method. The densities of both Fo and En were consistent to within 1% of the theoretical densities. The theoretical densities of composites were calculated from the densities of single crystal Fo and En and their volume fractions according to the following equation:

$$\rho_c = V_{Fo}\rho_{Fo} + (1 - V_{Fo})\rho_{En} \quad (1)$$

where V and ρ are the volume fraction and density, respectively; the subscript c denotes the composite; $\rho_{Fo} = 3221$ kg/m^3 and $\rho_{En} = 3198$ kg/m^3 (Bass, 1995). The initial porosities of samples were estimated to lie within the range of 0.5–1.2%.

Samples, for creep tests, were cut from the bulk hot-pressed samples and were rectangular in shape with typical dimensions of $3 \times 3 \times 6$ mm^3. Two end faces of the specimen, polished with 1 μm diamond paste, were optically reflective and parallel within 2 μm.

2.2. Experimental apparatus

The apparatus used is a high resolution 0.1-MPa creep rig, newly setup in the Laboratory of Tectonophysics, École Polytechnique de Montréal. Stress was applied via two silicon carbide (SiC) pistons, for which plastic deformation was negligible under the conditions of this study. Sample shortening was monitored using two linear variable differential transformers (LVDTs) attached to the pistons. The LVDT has a nominal full range of ±3.0 mm with a resolution of 0.2 μm. Temperature was monitored by two R-type (Pt/Pt–13% Rh) thermocouples located within 5 mm of the sample and could be controlled to ±0.5 K. Thermal profiling indicated that temperature gradients were less than 0.5 K /mm along vertical and horizontal directions. The oxygen fugacity (f_{O_2}) was varied by flowing a CO/CO_2 mixture with different ratios and monitored with a solid electrolyte, zirconia-based sensor. From the uncertainties in measuring displacement, load, sample dimensions, and temperature, the uncertainties in measuring stress and strain are estimated within ±0.1 MPa and ±0.01%, respectively, by applying the error propagating theory.

2.3. Experimental procedure

Deformation experiments were performed in a constant load mode (creep test) under the conditions of $T = 1423$–1593 K (0.78–$0.88T_m$ for En and 0.65–$0.73T_m$ for Fo), $P = 0.1$ MPa and $f_{O_2} = 10^{-14}$–$10^{-2.5}$ MPa. Applied compressive stresses (σ) were varied in the range of 18–100 MPa, yielding strain rates ($\dot{\varepsilon}$) of

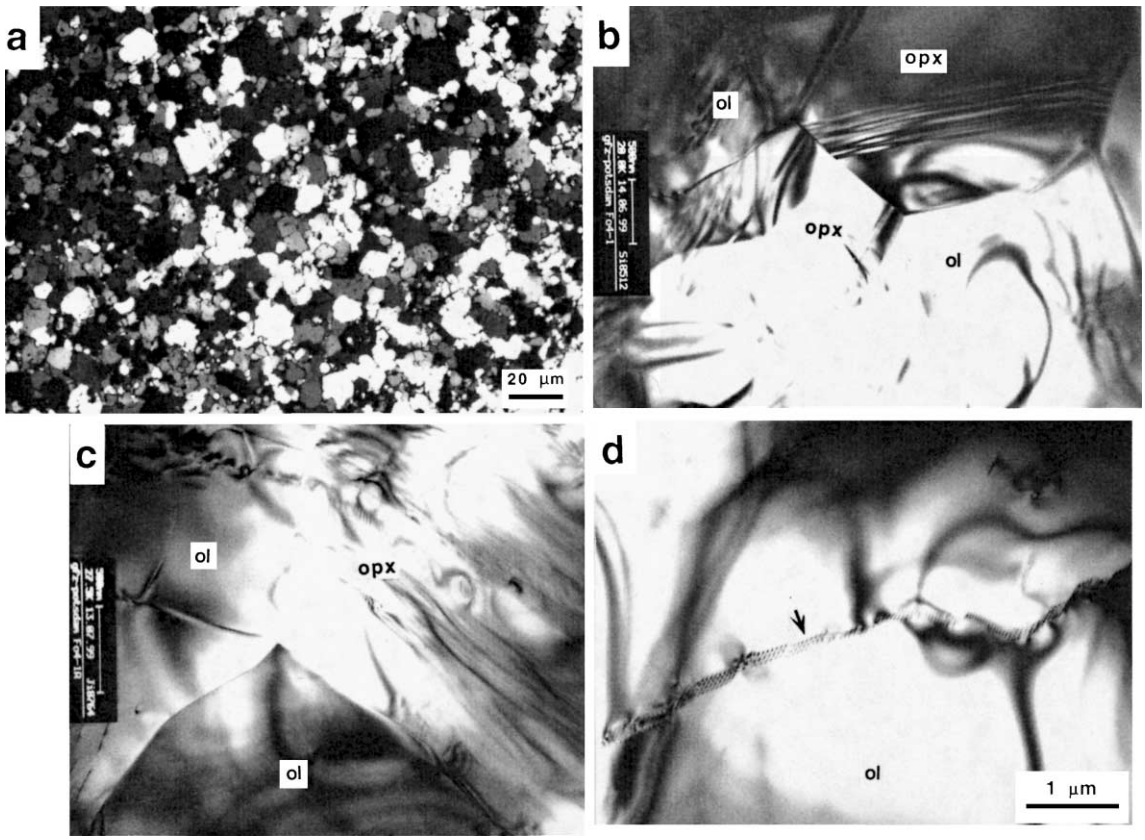

Fig. 1. Optical (a) and TEM micrographs (b–d) of undeformed, hot-pressed (a–b) and annealed (c–d) composite sample (Fo40: $V_{Fo}=40\%$). In (a), large grains are enstatite, small grains are forsterite. The sample has a foam texture with quasi-equilibrium grain boundaries and triple junctions. In (b) and (c), Fo/En, Fo/Fo, En/En grain boundaries are straight and free of inclusions or secondary phase. Twins occur in the En grains (Opx). Scattered distributed dislocation loops or short free dislocations can be seen in both Fo (Ol) and En (Opx) grains, but the average dislocation density is very low ($<2\times10^{-12}$ m^{-2}). (d) Dislocation walls (arrow) in an annealed Fo grain.

about 10^{-7}–10^{-4}/s. In the experiments, σ, T and f_{O_2} were varied in a stepwise manner to determine the dependency of the creep rate on those variables. To maintain constant σ, load was corrected periodically to accommodate changes of cross-section assuming a homogeneous plastic deformation. Creep data were collected from both transient and steady-state creep, but only the data obtained from steady-state creep were used for establishing the flow law. Steady-state creep rates were calculated from the creep steps with a total strain of 1.0–1.5% in each steady-state creep regime. The final strain of each sample was kept less than 10% to eliminate the uncertainty due to cavitation strain (see discussion in Section 2.4). A few samples were deformed to a total strain larger than 30% at fixed conditions to ensure that steady-state creep was indeed reached and that samples were deformed within the ductile regime. At least one step of every experiment was repeated to verify reproductivity of creep results. When identical σ, T and f_{O_2} conditions were repeated, strain rate values were usually in agreement. This reproductivity indicates that the sample microstructures (e.g., grain size and dislocation density) were almost identical under the same deformation conditions.

2.4. Data analysis

Microstructural analysis: About 200 μm surface layer was removed from the samples after the defor-

mation. The new surface was polished to 1 μm with diamond lapping film. To reveal grain boundaries, deformed samples were first chemically etched in acid ($HF:H_2O = 1:2$) at room temperature, then thermally etched at 1173–1273 K for 10–30 h. Optical microscopy and SEM were used to characterize grain size and texture of samples.

Mechanical data analysis: Previous studies of synthetic polycrystalline aggregates deformed in a similar 0.1 MPa rig indicated that cavitation strain becomes significant at creep strains larger than about 10% (Li et al., 1996; Kohlstedt et al., 2000). In this study, we also observed a decrease in density by 1–2% for samples deformed to total strain of ~10%, which we attributed to the cavitation. To remove cavitation effects from the creep data, we corrected all the data based on the theory and procedure proposed by Raj (1982):

$$\varepsilon_{\text{creep}} = \varepsilon_{\text{measured}} - \varepsilon_{\text{cavitation}} \quad (2)$$

where $\varepsilon_{\text{cavitation}} = 1/3\ (\Delta\rho/\rho_0)$, and $\Delta\rho$ is the difference in density ($\Delta\rho = \rho_0 - \rho$). Here the bulk densities before (ρ_0) and after deformation (ρ) can be measured precisely so that the strain rate can be corrected accordingly.

After correcting for the cavitation strain, the data of steady-state creep were analyzed using a flow law of the form:

$$\dot{\varepsilon} = A\sigma^n d^{-p} f_{O_2}^q \exp\left(-\frac{Q}{RT}\right) \quad (3)$$

where Q is the activation energy, A is a material parameter, and n, p and q are the stress, grain size (d) and oxygen fugacity exponents, respectively. In this study, the creep parameters such as n, Q and q were determined using multiple variable linear regression. The error in the best fit is given by the standard deviation.

3. Experimental results

3.1. Grain growth and microstructures of hot-pressed samples

One of the most pronounced microstructural features of the hot-pressed Fo–En composites is the grain size distribution. Grain size analysis, using the linear intercept method along two orthogonal tracings made on SEM images (one parallel to and the other perpendicular to the axis of cylindrical sample), showed a nearly log-normal distribution in grain size for both Fo and En in the hot-pressed monophase and composite aggregates (Fig. 2). It is noted that grain growth kinetics in Fo–En composites during the hot pressing depends strongly on V_{Fo} (Table 1). Substantial grain growth was observed during hot-pressing in both Fo and En monophase aggregates, resulting in average grain sizes of Fo and En of 16.5 and 30.5 μm, respectively. The grain growth rates for both Fo and En are slower in Fo–En composites than that in pure Fo and En aggregates. The average grain size of Fo in the hot-pressed composites ranges from 6.2 μm ($V_{\text{Fo}} = 80\%$) to 10.2 μm ($V_{\text{Fo}} = 20\%$) and that of En varies from 14.2 μm ($V_{\text{Fo}} = 80\%$) to 29.5 μm ($V_{\text{Fo}} = 20\%$). In a given composite, En grains are always larger than Fo grains by a factor of 2–3. The difference in grain growth kinetics between Fo and En yields two significant impacts on the textures of the synthesized composites: (a) bi-modal distribution of grain sizes with En grains larger than Fo ones in each composite (Fig. 2), and (b) likely difference in phase continuity between Fo and En for a given volume fraction.

Microstructural observations suggest that three microstructural regimes can be distinguished for the isostatically hot-pressed Fo–En composites in term of phase contiguity: (1) En phase is arranged in a continuous framework ($V_{\text{Fo}} \leq 0.4$) while Fo is isolated and dispersed in the matrix of En. The composite in this regime has the so-called WPS (weak-phase supported) structure which corresponds to the IWL (interconnected weak layer) structure defined by Handy (1994). (2) Fo phase is arranged in a continuous framework, whereas En phase is fully dispersed in the matrix of Fo ($V_{\text{Fo}} \geq 0.6$). The composite in this regime shows the so-called SPS (strong-phase supported) structure which is referred as the LBF (load-bearing framework) structure by Handy (1994). (3) Transitional regime ($0.4 < V_{\text{Fo}} < 0.6$), in which both En and Fo are topologically continuous and interconnected throughout the microstructure. This type of composite is an interpenetrating phase composite in the terminology of materials science (Clarke, 1992). The above classification is consistent with Gurland's (1979) concept of phase continuity and contiguity.

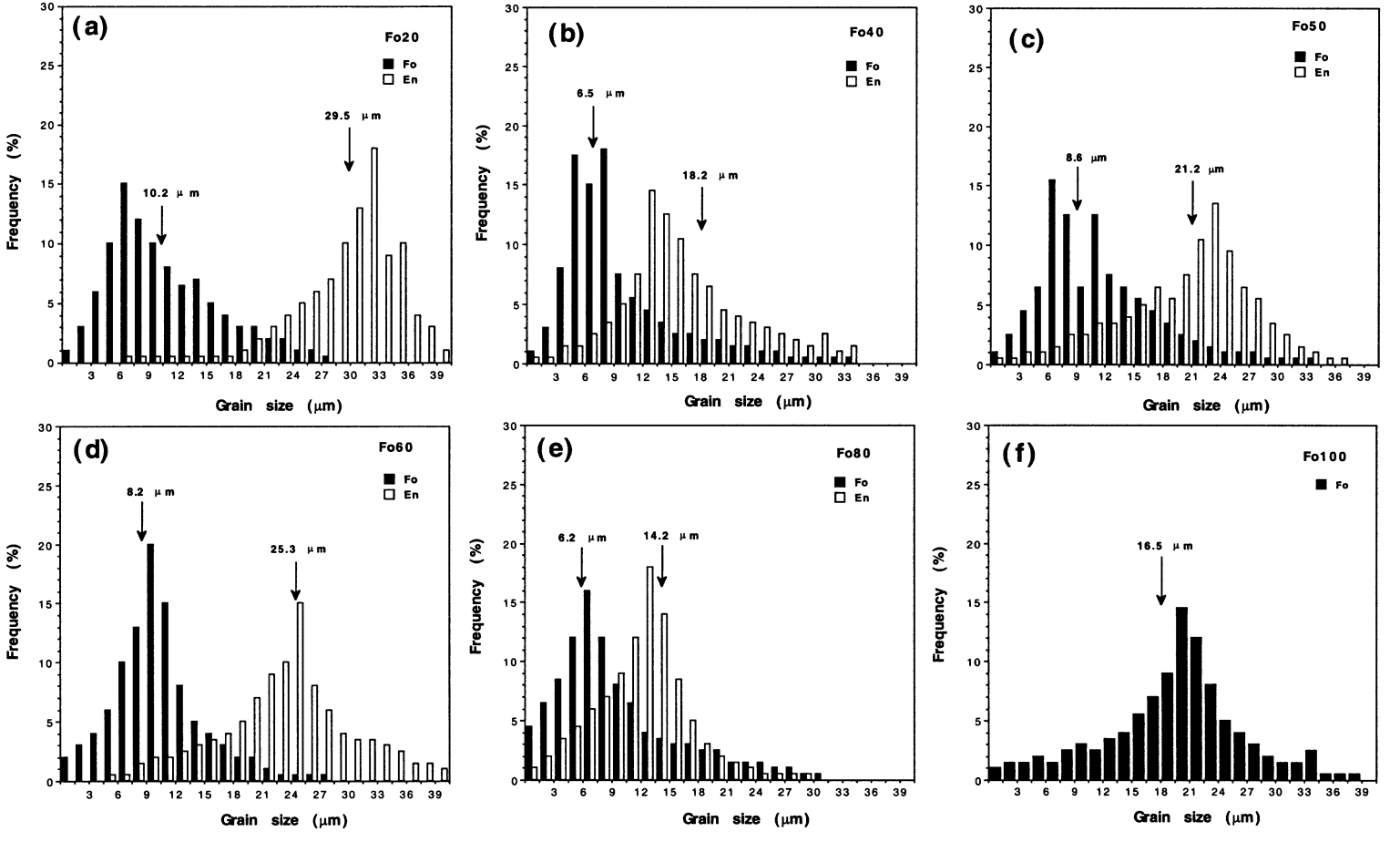

Fig. 2. Histograms showing the grain size distributions of Fo and En in the isostatically hot-pressed samples. The results show a nearly log normal distribution of grain size for both En and Fo grains. The mean grain sizes are indicated by arrows. Note that the average grain size of En is about a factor of 2–3 larger than that of Fo in the same composite. (a) Fo20En80; (b) Fo40En60; (c) Fo50En50; (d) Fo60En40; (e) Fo80En20; (f) Fo100En0.

Table 1
Fo–En composite samples and deformation conditions

Sample	V_{Fo}	Experimental conditions			Grain size (μm)[a]	
		T (K)	σ (MPa)	$\log(f_{O_2})$ (MPa)	Fo	En
Fo100-1	1.0	1523	25–100	−2.5	16.5±2.5	
Fo100-2	1.0	1463–1580	50	−2.5		
Fo80-1	0.8	1473–1593	26–79	−2.5	6.2±1.5	14.2±2.5
Fo80-2	0.8	1505–1551	32–74	−2.5		
F080-3	0.8	1503	45	−14.0 to −2.5		
Fo60-1	0.6	1523	33.1–59	−2.5	8.2±3.5	25.3±3.5
Fo60-2	0.6	1486–1580	33.5–45	−14.0 to −2.5		
Fo60-3	0.6	1503	18–75	−2.5		
Fo50-2	0.5	1423–1541	41–73.5	−2.5	8.6±2.5	21.2±4.5
Fo50-3	0.5	1486–1616	35–69	−2.5		
Fo50-3	0.5	1503	45	−14.0 to −2.5		
Fo40-1	0.4	1488–1573	28–68	−2.5		
Fo40-2	0.4	1497–1573	33–41	−2.5	6.5±1.5	18.2±3.0
Fo20-1	0.2	1523	18.5–76.1	−2.5		
Fo20-2	0.2	1498–1558	47	−14.0 to −2.5	10.2±1.5	29.5±3.5
Fo20-3	0.2	1503	26.6–59	−2.5		
En100-1	0.0	1483–1555	45	−2.5		30.5±4.5
En100-2	0.0	1503	31.3–80	−2.5		
En100-3	0.0	1503	45	−14.0 to −2.5		

[a] Grain size after isostatic hot press.

3.2. Mechanical data

3.2.1. Creep curves

Two-stage creep (i.e., transient and steady-state creep) was generally observed for the Fo–En composites. The composites with $V_{Fo} < 80\%$ showed a markedly transient creep regime during which the strain rate decreases with time (Fig. 3). Steady-state creep was reached only after a certain amount of transient strain ($\sim 0.1-1.1\%$). Under the conditions of our experiments, most of the Fo–En composites showed completely ductile behavior and no creep acceleration was observed even at total creep strain as high as 30%.

3.2.2. Effect of stress on creep rate

Fig. 4 shows the steady-state creep rates as a function of the applied stress for the Fo–En composites deformed at 1523 K and in air. For each individual sample, measured creep rates show a linear dependence on stress in $\log\sigma - \log\dot{\varepsilon}$ space, suggesting the operation of a single creep mechanism (Poirier, 1985). However, the slopes of fitting lines which give the stress exponent (n), decrease quasi-linearly with V_{Fo} from $n=2.0$ (Fo0) to $n=1.3$ (Fo100) (Fig. 4b). This trend indicates an increase in the contribution of diffusion creep to the bulk plastic deformationof the Fo–En composites with V_{Fo} (also see Table 2).

Forsterite: The creep rates, measured at $\sigma = 15.0-85.0$ MPa, varied from 1.67×10^{-7} to 4.84×10^{-7}/s with n of 1.3±0.3.

Enstatite: The creep rates, measured at $\sigma = 20-90$ MPa, varied from 1.89×10^{-6} to 1.32×10^{-5}/s, with n=2.0±0.2.

Fo–En composites: The creep rates, measured as a function of stress over the range of $\sigma = 18.5-80.0$ MPa, varied from 2.11×10^{-7} to 1.03×10^{-6}/s. The n values were determined to be in the range of 1.5 ± 0.1(Fo80)–1.8 ± 0.2(Fo20), and increased almost linearly with decreasing in V_{Fo} (Fig. 4b).

3.2.3. Effect of temperature on creep rate

As shown in Fig. 5a, the creep rates of Fo–En composites are plotted as a function of temperature in $10^4/T - \log(\dot{\varepsilon})$ space to determine creep activation energy (Q). The plots are linear for the entire series of Fo–En composites.

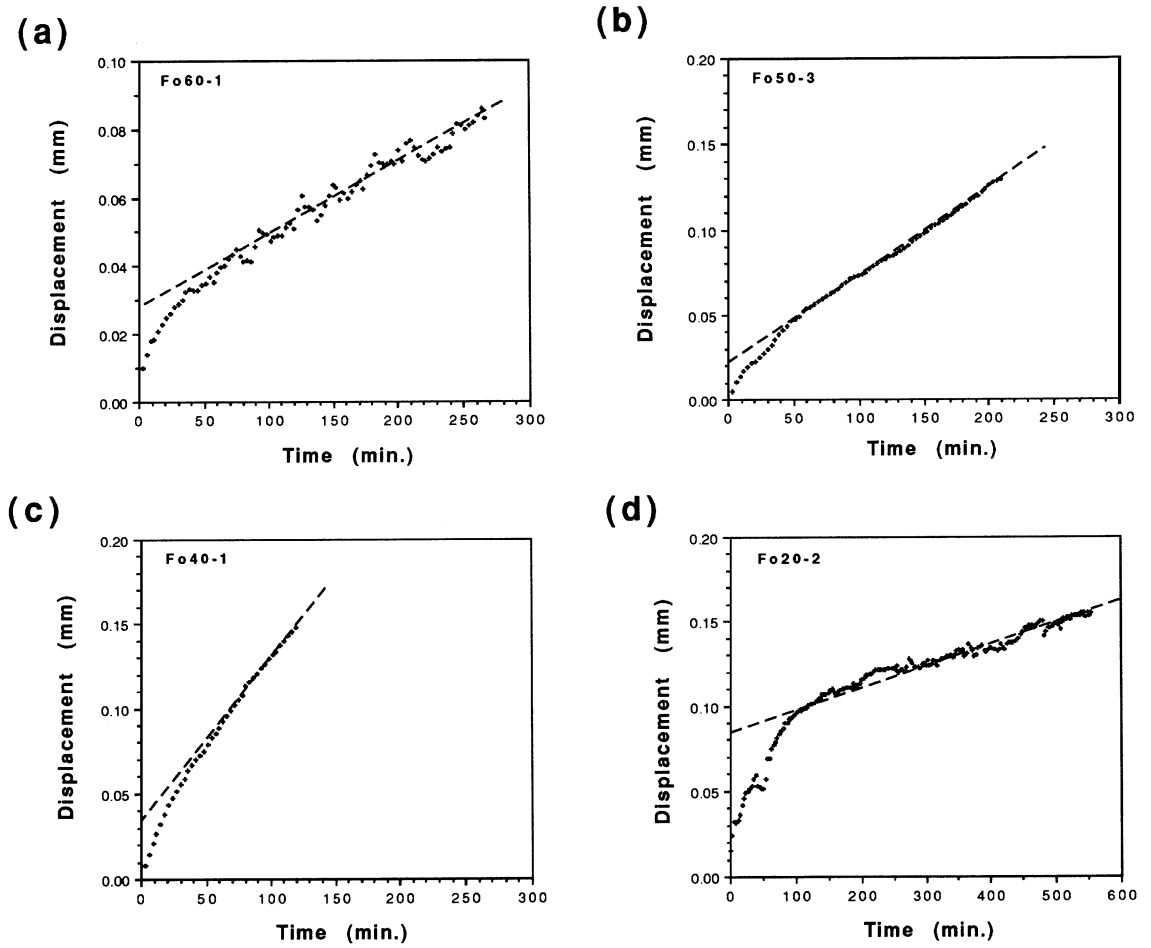

Fig. 3. Typical creep curves of the Fo–En composites showing both transient and steady-state creep. (a) Fo60-1, $T=1493$ K, $\sigma=45$ MPa; (b) Fo50-3, $T=1488$ K, $\sigma=45$ MPa; (c) Fo40-1, $T=1513$ K, $\sigma=45$ MPa; (d) Fo20-2, $T=1473$ K, $\sigma=40$ MPa.

Forsterite: The creep rates, measured at $T=1463$–1573 K and a fixed stress of $\sigma=45$ MPa, varied from 1.25×10^{-7} to 1.6×10^{-6}/s. Fitting the creep rates to Eq. (3) yields $Q=472\pm66$ kJ/mol.

Enstatite: The creep rates, measured at $T=1473$–1573 K, varied from 1.78×10^{-6} to 3.31×10^{-5} /s. Fitting the creep rate data to Eq. (3) yields $Q=584\pm24$ kJ/mol.

Fo–En composites: The dependence of creep rates on temperature are all linear in $10^4/T-\log(\dot{\varepsilon})$ space. The creep activation energies (Q) were determined to be within the range of 486 ± 19 kJ/mol (Fo80)–571 ± 28 kJ/mol (Fo20), showing linear decreases with increasing V_{Fo} for the composites with either WPS or SPS structure although a non-linear decrease for the transitional regime ($0.4<V_{Fo}<0.6$) (Fig. 5b).

3.2.4. Dependence of creep rates on f_{O_2}

Creep rates were measured as a function of f_{O_2} for two composites (Fo20 and Fo60) and a pure En aggregate (Fo0) under the conditions of $T=1523$ K, $\sigma=45$ MPa. The results showed that the creep rates of Fo0, Fo20 and Fo60 were almost independent of f_{O_2} for oxygen partial pressures higher than 10^{-14} MPa (Fig. 6). Similar behavior was previously reported on pure forsterite single crystals (Jaoul et al., 1980; Ricoult and Kohlstedt, 1985).

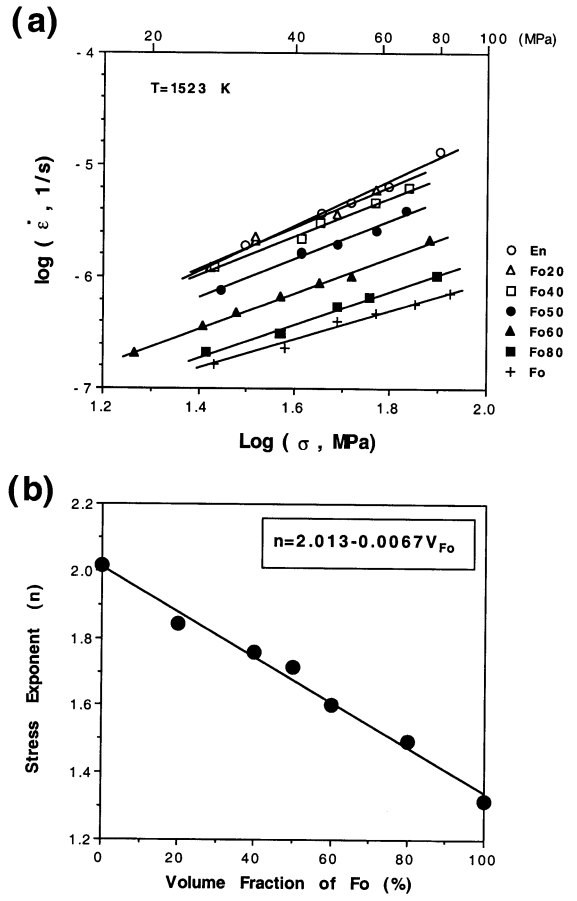

Fig. 4. (a) Log–log plots of strain-rates versus flow stresses at steady-state creep. The lines show the results of linear fits using least-square method and the slope of each line gives the stress exponent (n). The uncertainty is smaller than the size of the symbols. (b) The stress exponent (n) of the aggregates decreases almost linearly with the volume fraction of Fo.

3.2.5. Variation of composite creep strength with composition

The variation of composite flow stress with V_{Fo} was investigated by re-plotting the creep data at constant strain rate (10^{-6}/s) and two temperatures (1473 and 1573 K) using the rheological parameters of the Fo–En composites listed in Table 2. As shown in Fig. 7a, the En monophase aggregate has a weaker creep strength than that of Fo in the temperature range investigated. The bulk strength of Fo–En composites shows a non-linear dependence on the V_{Fo}. This non-linear rheological behavior of the composites is also clear in a plot of the creep rates normalized between the Fo and En end-members versus V_{Fo} at constant stress and temperature (Fig. 7b). The normalized creep rate is defined as $(\dot{\varepsilon}_c - \dot{\varepsilon}_{En})/(\dot{\varepsilon}_{Fo} - \dot{\varepsilon}_{En})$, where the subscript c denotes the composites.

3.3. Deformation microstructures

We used two samples with different lengths, the longer one subjected to deformation and the shorter one to annealing, during each run. This technique allowed us to investigate microstructures for both undeformed and deformed samples which had the same thermal history. Compared with the undeformed samples, the deformed samples show optically curved grain boundaries and heterogeneous undulatory extinction and slightly flattened Fo and En grains (Fig. 8). TEM observations showed that the undeformed composite samples developed static annealed structures such as well-organized dislocation walls and networks (Fig. 1d). These static annealed structures are believed to be generated during the hot-pressing. The free dislocation density is everywhere low ($<1\times10^{12}$/m^2) in both Fo and En grains and no sign for dislocation multiplication was observed in the annealed samples (Fig. 1c–d).

No significant differences in the dislocation microstructures were seen in the deformed samples with different Fo volume fractions. Figs. 9 and 10 are TEM microphotographs showing dislocation structures typical of the En and Fo grains in the deformed composite samples. Dislocations in Fo include long and straight or curved segments and dislocation walls or networks (Figs. 9 and 10). The straight dislocations are aligned in one or even two directions. Generally, the large grains have well formed low-angle subgrains and high dislocation densities while the small grains consistently have a lower dislocation density (Fig. 10a). The average dislocation density in Fo grains is about $6.5\pm3.5\times10^{12}$/m^2 with the highest value up to 5×10^{13}/m^2 observed in some grains. Small (<50 nm) bubbles (fluid inclusions?) were occasionally observed along some dislocation arrays and subgrain boundaries, although Fourier transform infrared spectroscopy analyses indicated that the deformed samples are typically dry because sharp peaks representative of O–H stretching frequencies are absent in the spectra. In addition, low dislocation density domains with

Table 2
Rheological parameters for the Fo–En composites and their end-members

Sample	V_{Fo} (vol.%)	Experimental conditions		Rheological parameters		
		T (K)	σ (MPa)	log$A$ (MPa^n/s)	n	Q (kJ/mol)
En100	0	1473–1573	20.0–90.0	11.60±0.81	2.0±0.2	584±24
Fo20	0.2	1494–1563	30.0–65.0	11.38±1.01	1.8±0.2	571±28
Fo40	0.4	1480–1573	25.0–80.0	10.86±0.78	1.7±0.1	554±23
Fo50	0.5	1476–1541	41.0–75.0	10.25±0.73	1.7±0.2	538±38
Fo60	0.6	1473–1558	18.5–78.0	8.79±0.53	1.6±0.1	502±18
Fo80	0.8	1486–1580	25.0–60.0	8.13±0.68	1.5±0.1	486±19
Fo100	1.0	1463–1573	15.0–85.0	7.75±0.60	1.3±0.3	472±66

grain boundaries slightly convex towards grains with higher dislocation density are also observed occasionally in deformed Fo grains. Thus, the general microstructures support significant dislocation activities in Fo grains in both the Fo aggregates and the composites.

The most pronounced substructures in En grains of the deformed composites are twin or kink lamellae (Fig. 9a–b), most of which are believed to be of deformation origin due to their long-lenticular shape. These lamellae cause undulatory extinction on the optical scale and are abundant at the TEM scale. Most of the lamellae terminate abruptly at grain boundaries. Some lamellae seem to be related to stacking faults between partial dislocations (Kirby and Christie, 1977). We have observed dislocations that are rotated by twinning (or kinking) and others which terminate against twin planes, indicating that twinning and dislocation glide occurred simultaneously during creep. Dislocation substructures were difficult to investigate in detail because of elastic interactions between dislocations and twin lamellae. The interaction caused a superposition of dislocation contrasts with twin fringes. Where dislocations could be observed in En grains, they were short and curved, and the dislocation density was generally lower than in neighboring Fo grains (Figs. 9 and 10). In addition, dislocation walls and networks have been occasionally observed in En grains. The above observations suggest that En grains in the composites were deformed by a combination of mechanical twinning or kinking, dislocation glide and diffusion-accommodated recovery process.

Most of the like (Fo/Fo or En/En) and unlike (Fo/En) grain boundaries in the deformed samples are clean with no impurity phase (Fig. 9a–b). In general, dislocation density is obviously lower in regions near grain boundaries than it is in regions near phase boundaries (i.e., interfaces). This observation indicates either that stress is concentrated at interfaces or that the interfaces act as barriers to dislocation motion. In addition, dislocation density near interfaces is lower when dislocation lines are parallel than perpendicular to the interfaces. This observation suggests that interface-reaction of dislocations took place.

4. Discussion

4.1. Comparison with previous experimental results

To understand the rheological behavior of polyphase rocks, there have been many experimental studies on two-phases materials with end-members of distinct mechanical properties. Experiments using synthetic two-phases composites or natural polyphase rocks with end-members of relatively large strength contrasts have shown that most of the bulk sample strain is accommodated by plastic deformation of the weak phase, while the strong phase either deforms by brittle processes if it is volumetrically the major phase, or acts as rigid inclusions and contributes relatively little to the bulk sample strain (e.g., naphthalene-ice and camphor-ice systems: Burg and Wilson, 1987; calcite–halite composites: Jordan 1987, 1988; anhydrite–halite: Ross et al., 1987; quartzo-feldspathic rocks: Dell'Angelo and Tullis, 1996; anorthite–quartz composites: Ji et al., 1999, 2000; quartz–mica composites: Tullis and Wenk, 1994; calcite–quartz, Dresen et al., 1998; olivine–basalt: Hirth and Kohlstedt, 1995). As shown by Ji and Zhao (1994) and Zhao and Ji (1997), experimental data on two-phase rocks with phases of relatively high strength contrasts (>5)

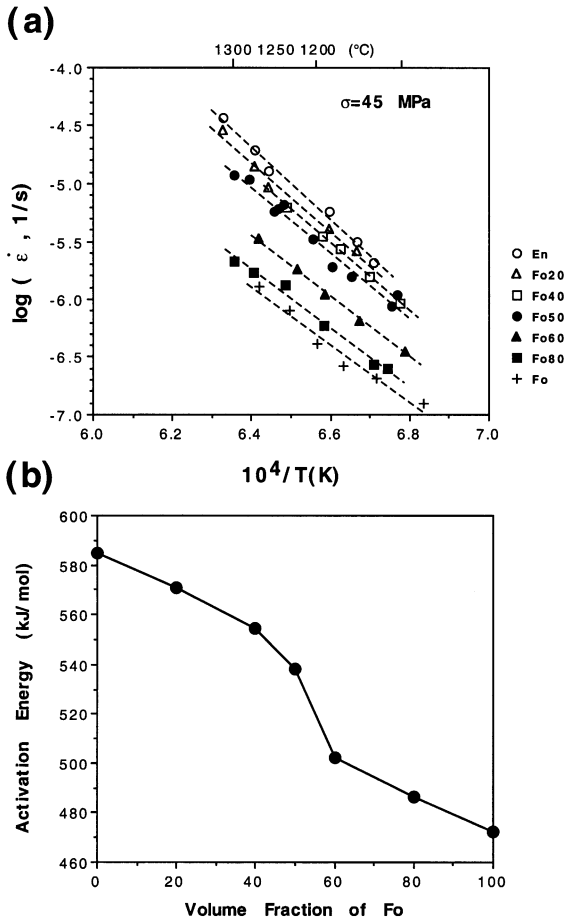

Fig. 5. (a) Semi-log plots of strain-rate versus temperature [$\log(\dot{\varepsilon}) - 1/T$]. Experimental data were normalized to $\sigma = 45$ MPa, using the stress exponents n from Table 2. The dashed lines show the results of linear regression using the least-square method and the slopes give activation energies (Q). The uncertainty is smaller than the size of the symbols. (b) The variation of activation energy as a function of V_{Fo}.

are generally consistent with the prediction of the shear-lag (fiber-loading) model (Kelly and Macmillan, 1986).

Depending on the deformation conditions such as temperature, pressure and strain rate, two-phase rocks may consist of phases with small strength contrast and thus more than one phase may actively contribute to the bulk deformation (e.g., plagioclase–pyroxene in diabase: Kronenberg and Shelton, 1980; Mackwell et al., 1998; pyroxene–olivine in peridotites: Hitchings et al., 1989; Daines and Kohlstedt, 1996; Lawlis, 1997; calcite–anhydrite: Bruhn et al., 1999). As pointed out by Tullis et al. (1991), most natural silicate rocks will fall into this category under natural deformation conditions. Olivine–pyroxene rocks, which are dominant in the upper mantle, provide one good example for study.

The present investigation provides a new set of creep data on Fo–En composites under dry conditions. Olivine–pyroxene composites have been studied by a few research groups previously (Hitchings et al., 1989; Daines and Kohlstedt, 1996; Lawlis, 1997; McDonnell et al., 2000), but their sample compositions and water contents, and the experimental scopes and apparatus were different from ours. Most of the previous studies used Fe-bearing olivine–pyroxene aggregates with Fe/(Mg + Fe) ≈ 10% in both olivine and pyroxene components.

Hitchings et al. (1989) investigated the rheology of fine-grained (10–38 μm) olivine–pyroxene aggregates at a confining pressure of 300 MPa and a temperature of 1500 K. The bulk stress exponent (n) is close to 3, implying that the composites deformed in the regime of dislocation creep. Using orientation contrast, forward-scattered SEM images, Fliervoet et al. (1999) examined one of the samples (Sample 5072 with total strain of ~20%) deformed by Hitchings et al. (1989) and found

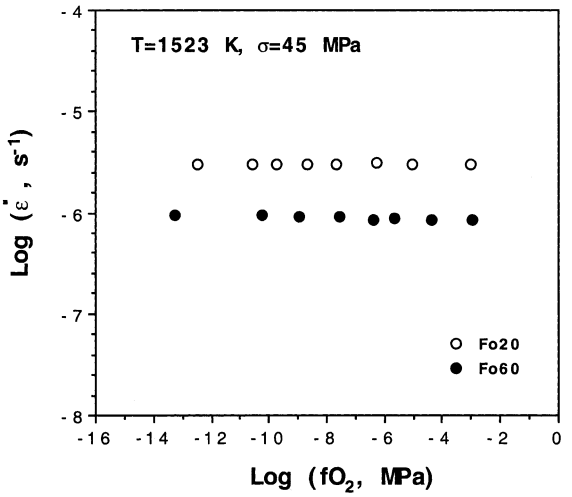

Fig. 6. Log–log plots showing strain-rates as a function of f_{O_2} at $T = 1523$ K and $\sigma = 45$ MPa. No clear dependence of the strain-rate on f_{O_2} was detected.

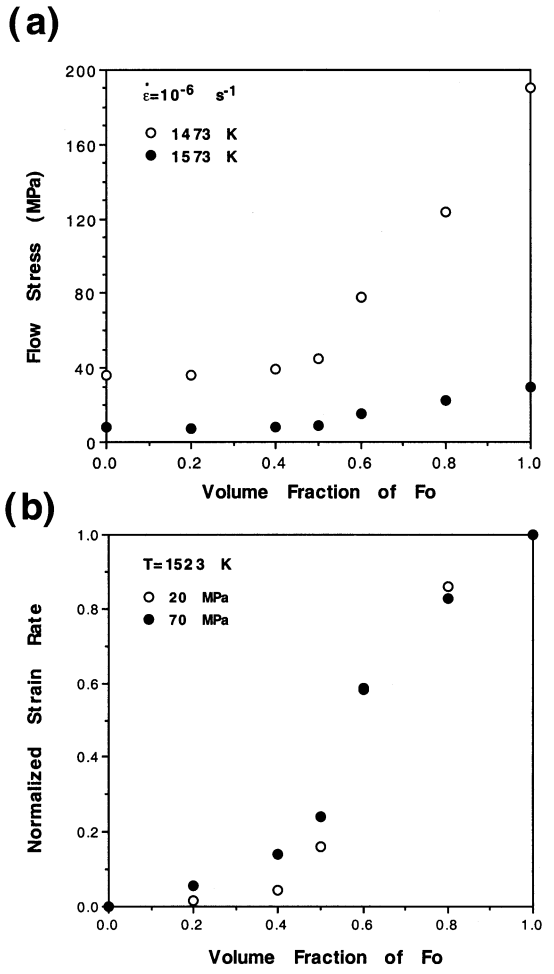

Fig. 7. Plots showing the creep strength as a function of V_{Fo}. (a) Absolute creep strength is plotted against V_{Fo} at $\dot{\varepsilon}=10^{-6}$/s, $T=1473$ and 1573 K. (b) Normalized creep strain-rates are plotted against V_{Fo} at $\sigma=20$ MPa and $\sigma=70$ MPa at $T=1523$ K. Non-linear dependencies of creep behavior on V_{Fo} are observed in both (a) and (b).

that this sample is characterized by larger grains ($\sim$13 μm) surrounded by smaller recrystallized grains ($\sim$5 μm). The larger grains show undulatory extinction and have subgrains and olivine develops a clear crystallographic preferred orientation with its *b*-axis subparallel to the compression direction and *a*-axis in the plane perpendicular to the compression direction (Fliervoet et al., 1999). Hitchings et al. (1989) reported that the composite samples were weaker than the end-members. It is difficult to interpret such a rheological weakening for a two-phase mixture in which each phase deforms by dislocation creep as it does in a single-phase aggregate.

A similar phenomenon was observed recently for fine-grained (2–4 μm) calcite–anhydrite (50:50) aggregates deformed at 827 K (Bruhn et al., 1999). For their grain sizes and experimental conditions, each phase deformed dominantly by diffusion creep whenever in the composite or in the single-phase aggregate. Based on previous studies (Wheeler, 1992), Bruhn et al. (1999) interpreted their results as due to enhanced boundary diffusion rates between unlike phases relative to like phases.

Daines and Kohlstedt (1996) deformed an olivine–enstatite aggregate with a composition similar to that of Hitchings et al. (1989) in the diffusion creep regime ($n=1.2$) at a confining pressure of 300 MPa, temper-

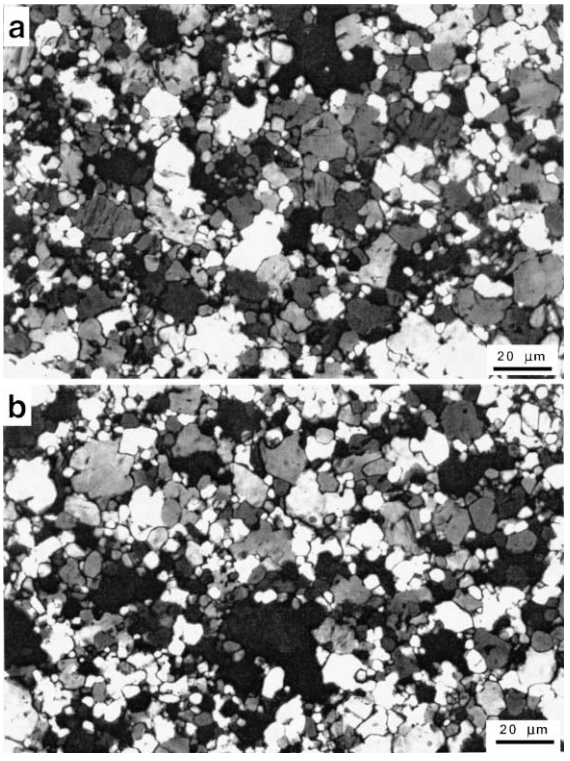

Fig. 8. Optical micrographs of a deformed Fo–En composite consisting of 40 vol.% forsterite (sample Fo40-2). Curved grain boundaries and undulatory extinction due to lattice bending and kinking are the main optical evidence for plastic deformation of both Fo and En grains. (a) Thin section cut perpendicular to σ_1 and (b) thin section cut parallel to σ_1.

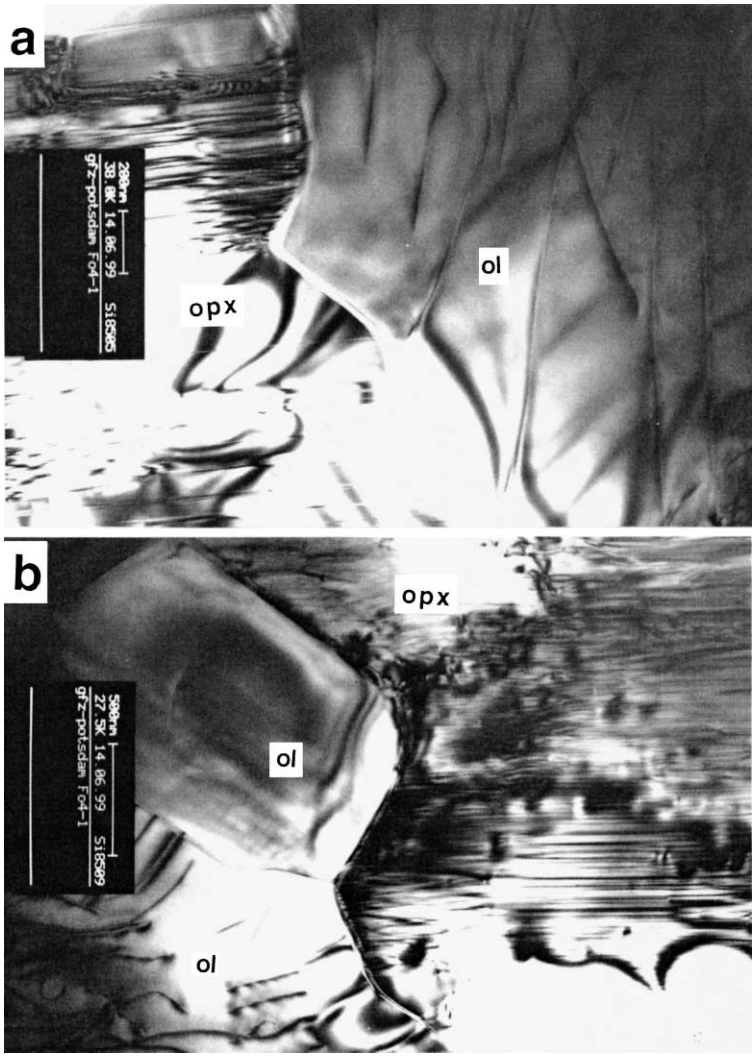

Fig. 9. (a and b) TEM micrographs (bright field) showing the typical deformation microstructures in Fo and En grains in deformed composite sample Fo40-1. The En grains are characterized by mechanical twinning or kinking and short dislocations while the Fo grains by high density of relatively straight, long dislocations.

atures between 1423 and 1528 K and strain rates between 10^{-7} and 10^{-5}/s. They observed little change in flow stress for composites containing 5%, 50% and 95% enstatite. Their experimental results disagree with the earlier suggestion of Hitchings et al. (1989). Lawlis (1997) recently performed a systematic study on the rheological behavior of olivine–pyroxene aggregates at $P=300$ and 450 MPa and $T=1423-1573$ K. Most of his experiments were conducted in the dislocation creep regime with $n=3-3.5$ and $Q=540-720$ kJ/mol. His results, also in contrast with those of Hitchings et al. (1989), showed a linear dependence of $\log \dot{\varepsilon}$, n and Q on V_{En}.

McDonnell et al. (2000) experimentally deformed wet (0.5 wt.% water) Fo–En composites with En contents of 0%, 1%, 2%, 2.5%, 15% and 20% and extremely small grain sizes (1–2 μm) using a gas-medium deformation apparatus at temperatures of 1173–1273 K, strain rates between 10^{-7} and 10^{-5}/s and a confining pressure of 600 MPa. They observed a

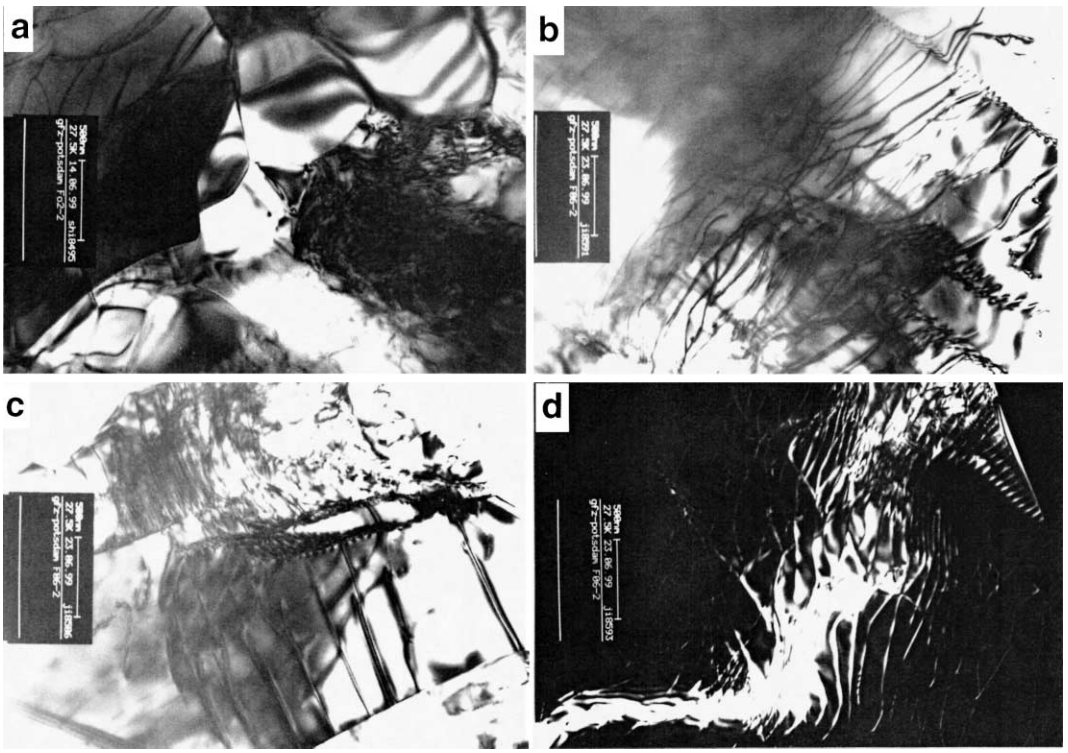

Fig. 10. TEM micrographs (a–c: bright field; d: dark field) showing the typical dislocation substructures in Fo grains from deformed composite samples Fo20-2 (a) and Fo60-2 (b–d). In (a), a higher density of dislocations usually occurs in larger grains than in smaller grains. Dislocation walls (b and d), cells (c) and networks indicate activities of dislocations.

sharp drop in composite flow strength with increasing En content from 0 to 2.5% and little further change at higher En contents up to 20 vol.%. Based on the observed stress exponent n value of ~ 1.7, grain size exponent p value of ~ 3 and microstructures, McDonnell et al. (2000) suggest that the deformation mechanism of their composite samples was grain boundary sliding accommodated by grain boundary diffusion and/or dislocation activity. Their mechanical data are inconsistent with the expectation for enhanced diffusion along unlike phase interfaces of the type proposed by Wheeler (1992) and Bruhn et al. (1999). McDonnell et al. (2000) suggested that the observed drop in Fo–En composite flow strength resulted from a decrease in grain size due to inhibition of grain growth by the presence of the second phase. However, the p value was poorly constrained by McDonnell et al. (2000) owing to the fact that the mean grain size of their samples varied over an extremely narrow range (from 1 to 2 μm). Furthermore, the concept of grain size exponent (p) was established initially for monophase aggregates (Poirier, 1985) and probably cannot be directly applicable to polyphase systems. In our view, the physical meaning of p has not been clear for polyphase aggregates.

Our experiments were performed on Fe-free Fo–En composites in a 0.1-MPa creep rig to minimize the effect of chemical composition and water content on composite deformation, and to maximize the resolution of mechanical data. Such experiments provide several advantages over experiments performed on Fe-bearing composites at higher confining pressure: (1) Avoid the complication in creep behavior due to the addition of Fe because Fe plays an important role in governing point defect chemistry and thus solid state diffusion and kinetic properties. (2) With the high resolution of stress (± 0.1 MPa), strain measurement ($\pm 0.01\%$) and temperature (± 0.5 K), creep experiments can be performed

at a low stresses similar in magnitude to those producing flow in the upper mantle. (3) Experiments can be performed over a relatively wide temperature range, which is necessary for the precise determination of Q value corresponding to a given deformation mechanism (Fig. 5a). (4) A dry environment can be easily provided, a situation difficult to attain in experiments carried out in a high-pressure vessel. (5) The oxygen fugacity dependence of creep rate can be easily measured in detail.

However, three factors may affect the quality of the data obtained with the 0.1-MPa rig. First, without confining pressure, cavities develop in polycrystalline samples due to local tensile stresses that arise due to grain boundary sliding (Lange et al., 1980; Tsai and Raj, 1982). Second, without confining pressure, microfractures can form in these materials deformed to large strain in dislocation regime or in those deformed by grain boundary sliding. To minimize these effects, the total strain was limited to less than 10%, and the mechanical data were corrected for cavitation strain with the theory of Raj (1982). To confirm the reliability of the mechanical data, an inter-laboratory comparison was made on forsterite (Fig. 11), for which both single and polycrystal data are available under similar experimental conditions. Our data on Fo polycrystals are within those for the $[110]_c$ and $[101]_c$ orientations on single crystal forsterite (Darot and Gueguen, 1981), which define the strongest and weakest orientations, respectively, for forsterite crystals. Our mechanical data are also comparable to the Fo-aggregate data from Relandeau (1981) within experimental uncertainty. Third, the concentration of water or water-related species in minerals such as forsterite and enstatite generally increases with the confining pressure (Paterson, 1989 for a review). It is widely observed that a single-phase aggregate or a two-phase composite has a significantly higher creep strength in the 0.1 MPa rig than in the 300-MPa gas-medium apparatus (Xiao, 1999). This phenomenon is well known to result from the effects of water weakening. Thus, one should be cautious when directly extrapolating the creep data obtained from the 0.1-MPa rig to the upper mantle which deforms at significantly higher pressures and also water fugacities.

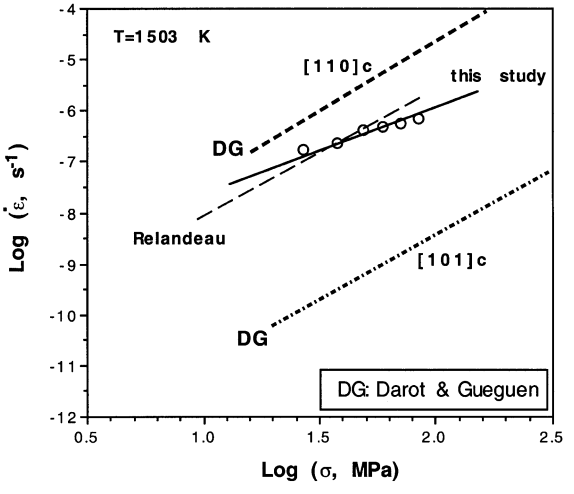

Fig. 11. Comparison of the results of Fo aggregates from this study with those obtained previously on forsterite single crystals and polycrystals. The data are plotted in $\log(\sigma)-\log(\dot{\varepsilon})$ space at $T=1503$ K. Single crystal data are from Darot and Gueguen (1981), and polycrystal data from Relandeau (1981). Open circles represent the data from this study and the solid line is the result of the best fit.

4.2. Deformation mechanism of the Fo aggregates

Previous experiments on polycrystalline olivine aggregates have demonstrated that both grain size sensitive (diffusion creep) and grain size insensitive (dislocation creep) behaviors can occur at confining pressures (P) from 0.1 MPa to 15 GPa and temperatures (T) up to 1873 K and that the transition between these two regimes depends mainly on grain size, temperature and water content. Our mechanical data on Fo aggregates can be fit well by a straight line on an Arrhenius plot, suggesting that a single mechanism is operating with $n=\sim 1.3$ and $Q=\sim 472$ kJ/mol (Figs. 4a and 5a). Although the n value is close to unity and suggests diffusion creep as the dominant deformation mechanism, abundant dislocation substructures are also observed throughout thin foils of deformed samples. Moreover, the measured creep activation energy of Fo aggregates is much larger than those for volume diffusion of oxygen, silicon and magnesium in forsterite (Jaoul et al., 1980, 1981; Chakraborty et al., 1992; McDonnell et al., 2000), but lower than the Q (571–730 kJ/mol) for dislocation creep of single crystals (Darot and Gueguen, 1981; Mackwell and Kohlstedt, 1986). Consequently, the Fo aggregates were most likely deformed by a mechanism which combines

volume diffusion of the slowest moving atomic species with formation and ionization of kinks or jogs on dislocation lines (Poirier, 1985). This mechanism can be referred as dislocation-accommodated diffusion creep.

The olivine aggregates and olivine–pyroxene composites hot-pressed and/or deformed with added water, which were previously reported to be deformed by a single mechanism of grain boundary diffusion creep (e.g., Chopra, 1986; Karato et al., 1986), probably contain melt which occurs in three- and four-grain junctions and wets at least parts of the two-phase boundaries (Wirth, 1996; Drury and Fitz Gerald, 1996). Using an internally heated gas-medium apparatus, Hirth and Kohlstedt (1995) successfully produced grain boundary diffusion creep in partially molten (< 12 wt.%) olivine–enstatite composites (olivine: Fo_{91}, 8.2–12.3 μm; enstatite: 3–5 wt.%, < 40 μm). On the basis of the above discussion, we speculate that volume diffusion creep accommodated by dislocation activity could be the dominant deformation mechanism in the melt-free Fo aggregates deformed under dry conditions. We do not intend to enter into any detailed discussion about interaction between volume diffusion creep and dislocation activity, as our main objective in this paper is to quantify the variations of the composite flow strength with the volume fraction of each constituent phase. The full determination of the dominant deformation mechanism in the deformed samples will be the topic for a separate research paper in the future.

4.3. Deformation mechanism of the En aggregates

Two pioneering studies examined the high temperature creep of natural enstatite-bearing rocks using a Griggs-type solid-medium apparatus at $P = 1.0$ and 1.5 GPa and $T = 1273–1673$ K (Raleigh et al., 1971; Ross and Nielsen, 1978). They both observed dislocation creep with $n = \sim 2.4–2.8$, and $Q = \sim 270–290$ kJ/mol. However, the sample assemblies used in their experiments during those earlier days did not allow stresses to be determined precisely. Recently, Lawlis (1997) studied synthetic, melt-free, fine-grained (1 to 20 μm) En-aggregates at $P = 300$ and 450 MPa, and $T = 1423–1573$ K. His samples were deformed in the dislocation creep regime with $n = \sim 2.9–3.0$ and $Q = \sim 600–720$ kJ/mol. We deformed pure En-aggregates in a similar range of temperature to that of Lawlis, and found that the rheological behavior can be described by a power-law creep with $n = \sim 2.0$ and $Q = \sim 584$ kJ/mol. Optical examination of the large En grains following deformation revealed undulatory extinction. TEM observations exclusively showed the dominance of mechanical twinning or kinking, dislocation glide and recovery. These observations suggest that the En grains deformed by a combination of mechanical twining or kinking, dislocation glide and diffusion-related recovery process.

4.4. Deformation mechanism of the Fo–En composites

Previous authors (e.g., McDonnell et al., 2000) suggested that the primary role of a secondary phase is to inhibit grain growth in a composite material, resulting in a relatively fine-grain size compared to end-member aggregates, promoting the transition from grain-size insensitive dislocation creep to grain-size sensitive diffusion creep. We also observed a significant reduction in grain size for both Fo and En in our composite samples (Table 1). For example, the mean grain size of Fo is 16.5 μm in the Fo aggregate as against 6.5 μm in the Fo40 composite. The mean grain size of En is 30.5 μm in the En aggregate as against 18.2 μm in the Fo40 composite. However, our TEM observations showed that the dislocation microstructures, including dislocation densities in either En or Fo individual grains, do not show significant variations with V_{Fo}, and are similar to those observed in pure Fo and En aggregates. This observation does suggest no change in deformation mechanism of each phase when in the composites, compared to when in a single-phase aggregate, for our grain sizes and experimental conditions. Whether in the composites or in the single-phase aggregate, the smaller grain-size Fo (6.2–16.5 μm) and the larger grain-size En (14.2–30.5 μm) crystals deform mainly by dislocation-accommodated diffusion creep and dislocation creep, respectively. Previous mixture rules (Tullis et al., 1991; Ji and Zhao, 1993), assuming that the mixing of two-phase phases does not change deformation mechanism of each phase, can account for fairly well the continuous decrease in n from 2.0 to 1.3 with increasing V_{Fo} from 0 to 1.0 (Fig. 4b). This interpretation is supported by the observed decrease in

Q from 584 to 472 kJ/mol with increasing V_{Fo} (Fig. 5b). The variation in Q, shown in Fig. 5b, may also suggest a continuous transition of the overall creep behavior of the composites from Fo-controlled rheology to En-controlled rheology. This transition may indicate that diffusion creep progressively gains dominance over dislocation creep in the composites with increasing V_{Fo}.

4.5. Comparisons with theoretical models

Modeling of the bulk strength of a polyphase composite material from the behavior of each end-member is an important and very active domain in modern materials science. During last three decades, many theoretical models have been developed and successfully applied to quantify the bulk strength of polyphase composites with various chemical compositions, microstructures and grain sizes. In this section, we will compare our creep results of Fo–En composites with theoretical models. Only analytical models have been selected for the comparison, complex numerical techniques such as finite element or finite difference modeling (e.g., Tullis et al., 1991; Bao et al., 1991) are not included. These latter techniques have advantages for comprehensively analyzing the effects of shape, concentration and spatial distribution of each phase and the influence of phase interface characteristics on the overall mechanical properties of two-phase composites, but they are too complicated to deal with when we have insufficient information about the detailed texture of the composites.

In order to facilitate the comparison between experimental data and theoretical models, we define a parameter K as normalized strength: $K=(\sigma_c-\sigma_{En})/(\sigma_{Fo}-\sigma_{En})$, where σ_{En} and σ_{Fo} are the flow strengths of the composite, Fo and En polycrystals, respectively.

4.5.1. Voigt, Reuss and Handy bounds

The simplest approach to composite bulk rheology is based on an assumption that the constituent phases of a composite undergo deformation characterized by either uniform strain rate (i.e., Voigt model) or uniform stress (i.e., Reuss model). The Voigt and Reuss models are generally thought to place upper and lower bounds on the overall flow strength for homogeneous and isotropic composites, respectively. Based on a notion that the rate of viscous strain energy dissipation in a polyphase rock is equal to the sum of the effective rates of strain energy dissipation in the constituent phases of that rock, Handy (1994) (corrected form) derived the following two bounds for composites with the LBF (load-bearing frame, SPS in our terminology) and IWL (interconnected weak layer, WPS in our terminology) microstructures:

$$\text{Upper bound}: \quad \sigma_c = \sigma_s V_s + \sigma_w(1-V_s) \tag{4}$$

$$\text{Lower bound}: \quad \sigma_c = \sigma_w(1-V_s)^{1-x} + \sigma_s[1-(1-V_s)^{1-x}] \tag{5}$$

where $x=(1-\sigma_w/\sigma_s)$, the subscripts c, s, and w stand for the composite, strong phase and weak phase, respectively. Handy's upper bound corresponds exactly to the Voigt bound while Handy's lower bound given by Eq. (5) is nearly the same as Reuss bound. As shown in Fig. 12a, these upper and lower bounds are separated widely and all the measured Fo–En composite strengths plot between these bounds. However, the measured data are close to the lower bound at $V_{Fo}\leq 0.20$ and to the upper bound at $V_{Fo}\geq 0.80$. At moderate V_{Fo} (0.40–0.60), neither upper nor lower bounds can fit the experimental data.

4.5.2. Takeda model

Recently, Takeda (1998) applied multiphase continuum mechanics to the flow properties of two-phase rocks. The analysis was based on assumed additive relationships for the linear momentum, stresses and entropy production rates. The low strength of Fo–En composites as a function of V_{En} or V_{Fo} can be calculated from Takeda's Eqs. (33) and (34) which correspond to his mode 1 and mode 2, respectively. His mode 1, which gives a linear relationship between the bulk composite strength and the volume fraction of the constituent phases, yields exactly the same composite strength as the Voigt bound. His mode 2 predicts a non-linear variation of the composite flow strength with the volume fractions, density contrast or rheological contrast between the two constituent phases. The density contrast and rheological contrast between Fo and En are about 1 (Ji and Wang, 1999), and 4.7 at $T=1503$ K and strain rate of 10^{-6}/s. As

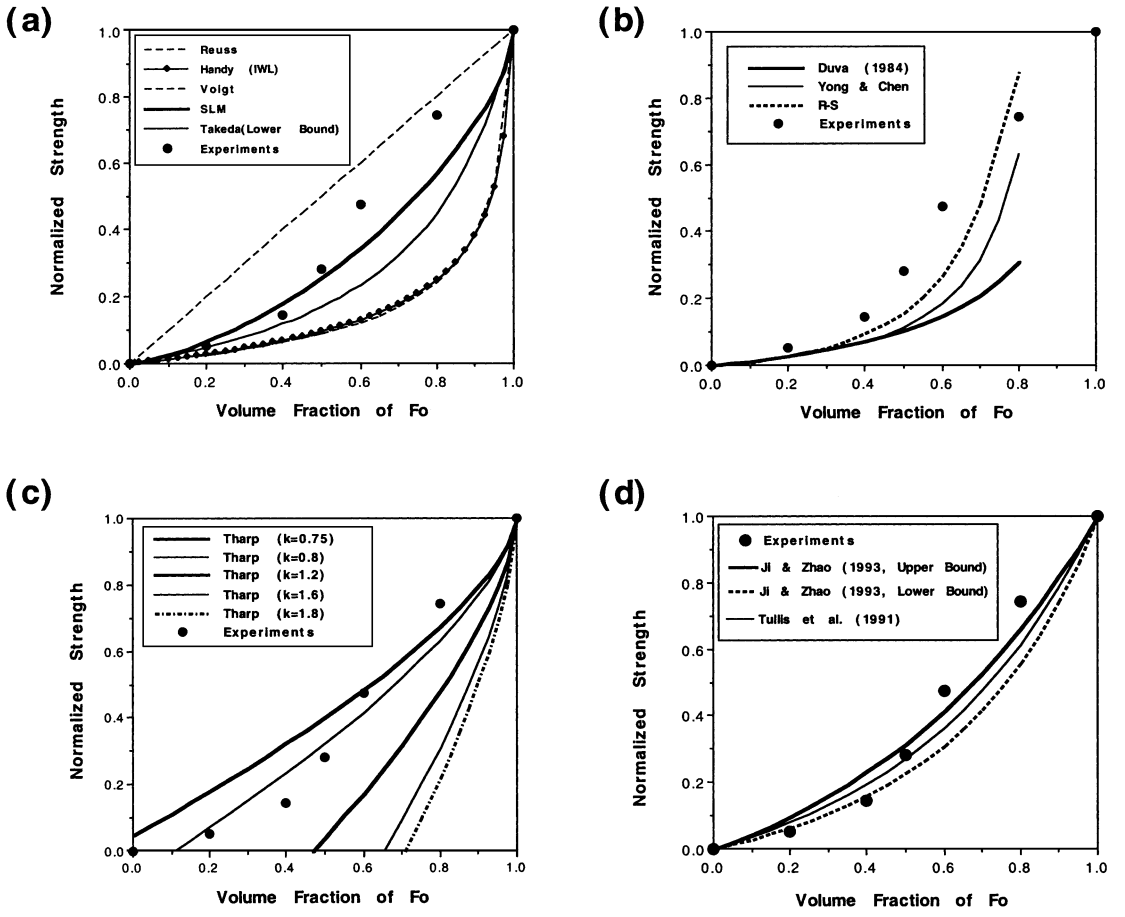

Fig. 12. Comparison of the experimentally determined flow strengths of Fo–En composites with those predicted from various theoretical models. The creep strength is normalized by strength contrast between Fo and En, and shown as a function of V_{Fo}. Solid circles are experimental data points; solid and dashed lines are the flow strengths predicted by various models. All data are normalized at $\dot{\varepsilon}=10^{-6}$/s, $T=1503$ K. (a) Reuss and Voigt bounds, shear-lag model (SLM), Handy lower bound, and Takeda (mode 2) model. (b) Duva model, Yoon–Chen model, and Ravichandran–Seetharaman (R–S) model; (c) Tharp model; (d) Tullis–Horowitz–Tullis empirical formulas and Ji–Zhao model.

shown in Fig. 12a, Takeda's mode 2 successfully predicts the flow strength of Fo–En composites with WPS structure at $V_{Fo} \leq 0.40$.

4.5.3. Shear-lag model

The shear-lag model (SLM) was originally proposed by Cox (1952) and subsequently refined by many others (Kelly and Macmillan, 1986; Zhao and Ji, 1997). The SLM has been widely used to predict elastic moduli (e.g., Ji and Wang, 1999) and yield strength (e.g., Kelly and Street, 1972; Nardone and Prewo, 1986) of composites. According to the modified SLM (Ji and Zhao, 1994; Hull and Clyne, 1996), the composite flow strength can be assessed by the following equation:

$$\sigma_c = (1 - V_s)\sigma_w + V_s\sigma_s\left[1 + \left(\frac{\sigma_w}{\sigma_s} - 1\right)\frac{\tanh\ \varphi}{\varphi}\right] \quad (6)$$

where

$$\varphi = s\left(\frac{-3\sigma_w}{\sigma_s(1+\upsilon_w)\ln\ V_s}\right)^{1/2} \quad (7)$$

where s is the average aspect-ratio of the strong phase ($s = \sim 1.5$ for Fo), and υ_w is the Poisson's ratio of the weak phase ($\upsilon_w = 0.208$ for En, measured by Ji and Wang, 1999). The flow strengths of the Fo–En composites calculated from the SLM are shown in Fig. 12a. The SLM prediction gives a fairly good approximation to the measured strength of composites with $V_{Fo} \leq 0.5$, however, a significant discrepancy between the theoretically predicted and experimentally measured values occurs at $V_{Fo} > 0.50$.

4.5.4. Duva model

Using a differential self-consistent analysis, Duva (1984) developed an approximate constitutive relation for a power-law viscous matrix material stiffened by rigid spherical inclusions:

$$\sigma_c = \sigma_w (1 - V_s)^{-0.48} \tag{8}$$

where σ_c is the overall flow stress of the composite in pure-shear, σ_w is the flow stress for the weak matrix without rigid inclusions, and V_s is the volume fraction of the rigid particles. Fig. 12b shows that the Fo–En composite strengths calculated from the Duva model match approximately with our experimental data only at $V_{Fo} < 0.3$. This result is not surprising because the Duva model does not take into consideration effects of particle clustering and is thus valid only for a composite material with a dilute distribution ($V_s < 0.3$).

4.5.5. Yoon–Chen model

Using a self-consistent approach, Yoon and Chen (1990) established a power-law relation between steady-state strain rate and stress for two-phase composites consisting of a soft creeping matrix reinforced by rigid inclusions. According to them:

$$\dot{\varepsilon}_c = A_w \sigma_c^{n_w} (1 - V_s)^q \exp\left(-\frac{Q_w}{RT}\right) \tag{9}$$

where $\dot{\varepsilon}_c$ and σ_c are the overall strain-rate and flow stress of the composite, respectively; A_w, n_w, and Q_w are the rheological parameters for the weak phase, V_s is the volume fraction of the rigid particles, and q is a parameter which describes the stress concentration due to the presence of the rigid particles and depends on n_w and the inclusion shape. For equiaxed inclusions, q is given by:

$$q = 2 + n_w/2 \tag{10}$$

(Yoon and Chen, 1990). This model predicts that the flow stress increase resulting from a given volume fraction of rigid inclusions is more drastic in a non-Newtonian creeping material than in a Newtonian material. Similar to the Duva model, the Yoon–Chen model gives a good prediction only when $V_{Fo} < 0.30$ (Fig. 12b). At higher V_{Fo}, both the Duva and Yoon–Chen models underestimate significantly the flow strength for Fo–En composites.

4.5.6. Ravichandran–Seetharaman model

Ravichandran and Seetharaman (1993) developed a simple continuum-mechanical model to predict the steady-state flow strength of two-phase composites containing coarse, rigid particles in plastically deforming matrix. The model was derived on the basis of a unit cell, representative of the composite microstructure, which is idealized to a pattern of periodic, cubic particles distributed uniformly in a continuous ductile matrix. The model accounted specifically for the constraints of rigid particles on plastic flow of the adjacent weak matrix (Unksov, 1961). According to the Ravichandran and Seetharaman model, we obtained the following flow law for our Fo–En composites:

$$\dot{\varepsilon}_c = A_{En} \exp\left(-\frac{Q_{En}}{RT}\right) \times \left[\frac{(1+c)^2 \sigma_c}{\left(1 + \frac{0.3}{c}\right)\left(1 + \frac{1}{c}\right)^{1/n_{En}} + (1+c)^2 - 1}\right]^{n_{En}} \tag{11}$$

where

$$c = (1 - V_{En})^{-1/3} - 1. \tag{12}$$

As shown in Fig. 12b, this model tends to underestimate the flow strength for the Fo–En composites with moderate $V_{Fo} = 0.30–0.70$. For the Fo–En composites, the Ravichandran–Seetharaman model is better than the Duva model, the Yoon–Chen model, the Reuss bound or the Handy model.

4.5.7. Tharp model

Instead of emphasizing the role of the weak phase, Tharp (1983) suggested that composites with a strong phase forming a SPS structure and a much weaker dispersed phase could be modeled as porous powder metals. According to him:

$$\sigma_c = \sigma_s(1 - kV_w^{2/3}) \tag{13}$$

where k is a geometrical coefficient which depends on a number of factors such as the shape and configuration of the weak phase and the strength contrast (σ_s/σ_w), and ranges from 0.98 to 3.8 (Griffiths et al., 1979). Tharp (1983) found that $k=1.8$ represents a good fit to empirical tensile strengths of various sintered porous metals, whereas Jordan (1987) found that $k=1.1-1.5$ for the compressional strengths of calcite–halite and anhydrite–halite. As demonstrated in Fig. 12c, the experimental data at $V_{Fo} \geq 0.60$ can be described by the Tharp model with $k=\sim 0.75$, which is lower than the values typically used by previous authors for other materials. As pointed out by Ji and Zhao (1994), the Tharp model cannot be applied to composites containing low to moderate volume fractions of strong phase (e.g., $V_s < 0.60$) because they generally cannot form a SPS structure.

4.5.8. Tullis–Horowitz–Tullis empirical formulas and Ji–Zhao bounds

One important consequence of the Voigt or Reuss (arithmetic) averaging is that the resultant composite creep data cannot be represented by a simple power law although the relation between flow stress and strain rate for each phase follows a power law. Given this restriction, Ji and Zhao (1993) proposed that the upper and lower bounds for the strength of multiphase composites can be obtained from a volume-weighted geometric average of the end-members under isostrain and isostress conditions, respectively. There are two advantages to this approach: (1) all the rheological parameters (n, A and Q) for the composite can be easily calculated (see Eqs. (4 to 6) and (9 to 11) in Ji and Zhao, 1993); and (2) the gap between the upper and lower bounds (Fig. 12d) is much smaller than that between the Voigt and Reuss bounds (Fig. 12a). Using a coefficient F which describes the state of strain rate or stress distribution among the constituent phases in the composite ($F=0$ for the uniform strain distribution and $F=1$ for uniform stress distribution), one can easily obtain a power law and its parameters for the multiphase composite through an iterative process (Ji and Zhao, 1993). As a particular case where a composite consists of only two phases and has $F=0.5$, the geometric averaging leads one to obtain the following equations:

$$n_c = 10^{(V_s \log n_s + V_w \log n_w)} \tag{14}$$

$$Q_c = \frac{Q_w(n_c - n_s) - Q_s(n_c - n_w)}{n_w - n_s} \tag{15}$$

$$A_c = 10^{[\log A_w(n_c - n_s) - \log A_s(n_c - n_w)]/(n_w - n_s)}. \tag{16}$$

These three equations were proposed as empirical formulas by Tullis et al. (1991) who are the forerunners for studying the rheology of two-phase rocks. They found that the flow strength of diabase containing 36 vol.% plagioclase and 64 vol.% clinopyroxene, predicted from Eqs. (14)–(16), agrees well with their results from finite element modeling. As shown in Fig. 12d, the Ji–Zhao lower and upper bounds seem to be a good approximation for the flow strengths of Fo–En composites with $V_{Fo} \leq 0.4$ and $V_{Fo} \geq 0.6$, respectively. At $V_{Fo}=0.5$, the Tullis–Horowitz–Tullis empirical formulas or the Ji–Zhao iteration with $F=0.5$ both predict composite flow strengths consistent with the experimental data.

4.5.9. Zhao–Ji model

Ravichandran and Seetharaman (1993) considered that the rheological behavior of a two-phase composite can be represented by the behavior of a basic unit cell containing one inclusion and the surrounding matrix. Stimulated by this idea, Zhao and Ji (1994) obtained the flow strength (σ_c) of the composite at a given strain rate ($\dot{\varepsilon}_c$), in which both the inclusion and matrix materials display power-law rheological

behaviors, by numerically solving the following two equations:

$$\sigma_c = (1 - V_i^{2/3})\left(\frac{\dot{\varepsilon}_c}{A_m \exp\left(\frac{-Q_m}{RT}\right)}\right)^{1/n_m} + V_i^{2/3}\sigma_{e2} \quad (17)$$

$$\dot{\varepsilon}_c = (1 - V_i^{1/3})A_m \sigma_{e2}^{n_m} \exp\left(\frac{-Q_m}{RT}\right) + V_i^{1/3} A_i \sigma_{e2}^{n_i} \exp\left(\frac{-Q_i}{RT}\right) \quad (18)$$

where the subscripts i and m stand for the inclusion and the matrix, respectively, and is the average stress of element 2 defined in Zhao and Ji (1994). The σ_{e2} value in Eq. (17) can be obtained from Eq. (18). A computer program for solving Eqs. (17) and (18) is available upon request from the first author. By alternatively taking i in Eqs. (17) and (18) to be Fo or En, we obtained the flow strengths of composites with WPS or SPS structures. In the WPS structure,

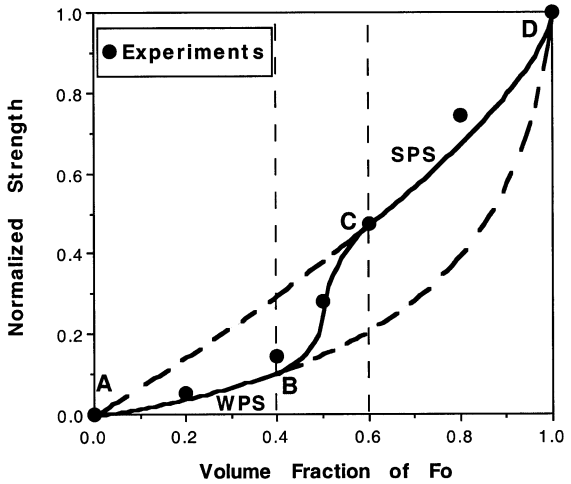

Fig. 13. Variations of flow strength of Fo–En composites with V_{Fo} in three structural regimes (WPS for $V_{Fo} < 0.4$, SPS for $V_{Fo} > 0.6$, and transitional regime for $V_{Fo} = 0.4–0.6$). The flow strengths of the composites with WPS and SPS structures can be approximately predicted by the Zhao–Ji model with Fo and En as inclusions, respectively. Curve BC is an empirical description for the transitional regime.

Table 3
Standard deviation of each theoretical model from measured data

Theoretical model	Standard deviation		
	$V_{Fo} \leq 0–0.4$	$V_{Fo} = 0.4–0.6$	$V_{Fo} \geq 0.6–1.0$
Takeda (mode 2)	±0.0146	±0.1486	Invalid
Ji–Zhao (lower bound)	±0.0165	±0.0991	Invalid
Shear-lag	±0.0167	±0.1457	±0.2281
Zhao–Ji (WPS)	±0.0233	±0.1715	Invalid
R–S	±0.0314	±0.1405	Invalid
Tullis–Horowitz–Tullis	±0.0333	±0.0709	±0.1069
Duva	±0.0393	±0.2174	Invalid
Yoon–Chen	±0.0419	±0.1979	Invalid
Ruess bound	±0.0440	±0.2327	±0.3972
Handy (lower bound)	±0.0587	±0.2648	±0.4680
Zhao–Ji (SPS)	±0.1016	±0.1062	±0.0522
Ji–Zhao (upper bound)	Invalid	±0.0632	±0.0642
Tharp ($k = 0.8$)	Invalid	±0.0651	±0.0859
Voigt bound	Invalid	±0.2071	±0.0762
Handy (upper bound)	Invalid	±0.2071	±0.0762
Takeda (mode 1)	Invalid	±0.2071	±0.0762

The smaller the number is, the better the model fits the experimental data.

Fo acts as inclusions in a matrix of En. In the SPS structure, however, En acts as inclusions in a matrix of Fo. Fig. 13 shows the calculated results using the measured flow law parameters of Fo and En from Table 2. It is important to note that there is a clear transition in creep behavior in the range of intermediate V_{Fo}. This transition is due to the transition from WPS ($V_{Fo} < 0.40$) to SPS ($V_{Fo} > 0.60$) structures.

4.5.10. Applicability of the models

To evaluate quantitatively the applicability of various theoretic models to predicting the composite flow strength in the WPS ($V_{Fo} < 0.40$), SPS ($V_{Fo} > 0.60$) and transitional ($0.40 \leq V_{Fo} \leq 0.60$) regimes, the standard deviation of each model from experimental data was calculated and the results are shown in Table 3. None of the existing models can fit the experimental data over the whole V_{Fo} range, although some of the models

match the experimental data well over a limited V_{Fo} range. In the WPS regime ($V_{Fo} < 0.40$), Takeda (1998) mode 2, Ji and Zhao (1993) lower bound, the shear-lag model, Zhao–Ji WPS model, and Yoon–Chen model provide relatively good assessments for the composite flow strength with the standard deviations < 3%. In contrast, the Reuss bound, Handy lower bound, Duva model and Ravichandran–Seetharaman model tend to underestimate the composite flow strength. In the SPS regime ($V_{Fo} > 0.60$), only Zhao–Ji SPS model and Ji–Zhao upper bound can predict approximately the composite flow strength with the standard deviations < 7%. These results are consistent with the assumptions and limitations of these theoretical models.

All the analytical models used to compare with our experimental data were based on an assumption that the overall mechanical behavior of the polyphase material can be adequately described by continuum constitutive equations governing balance of energy, compatibility of strain and stress, and balance of momentum. Actually, none of the models have taken into consideration changes in deformation mechanism of each phase due to mixing of the phases. As shown in Fig. 12, the general trends and even quantitative assessments of the bulk flow strength for the Fo–En composites with the WPS ($V_{Fo} < 0.40$) and SPS ($V_{Fo} > 0.60$) structures are successfully predicted by most of the theoretical models. Hence, the agreement between the theoretical models and our experimental results provides additional evidence supporting no change in deformation mechanism of each phase in the composite compared to in a single-phase aggregate. If there were such changes in deformation mechanism, none of the models could give good predictions for the composite flow strength over any range of Fo volume fraction.

The remaining problem is for composites in the transitional regime, for which practically no models have been developed. Using models based on either the WPS or SPS structure cannot yield a correct prediction for the composite strength in the transitional regime. The Fo–En composite is not a unique case; similar situations have been reported for a number of two-phase aggregates such as copper–WC alloy (Gurland, 1979) and calcite–halite aggregates (Bloomfield and Covey-Crump, 1993; Bruhn et al., 1999).

Rheology of composites in the transitional regime ($V_f = 0.4–0.6$) is complex and so far poorly understood. Many polyphase rocks in the Earth's crust (e.g., amphibolite, gabbro, diabase, mafic granulite) can be represented approximately by two-phase composites in which each phase is present in the 40–60 vol.% range. For example, gabbro, diabase, or mafic granulite often consists of plagioclase and pyroxene at nearly equal volume fractions. Knowledge of the creep properties of these rocks is important for understanding a wide range of tectonic processes in the ductile lower crust. Thus, there is a strong need to carefully characterize the microstructural evolution of polyphase rocks with progressive strain and to develop mechanical models with accurate descriptions of rheological behavior in the transitional regime. The mechanical modeling should take into account the following factors which are expected to affect the rheological behavior of polyphase rocks: (1) The nature of interfaces (boundaries between strong and weak phases) may affect the ease of interface slip (Ji et al., 1998), stress transfer between phases (Zhao and Ji, 1997) and chemical diffusion along grain boundaries (Wheeler, 1992; Bruhn et al., 1999). (2) Phase continuity may change with progressive strain (Gurland, 1979; Bloomfield and Covey-Crump, 1993; Dell'Angelo and Tullis, 1996). (3) Change of the dominant deformation mechanism and reversal of rheological contrast between phases with deformation conditions (Tullis et al., 1991; Dell'Angelo and Tullis, 1996; Bruhn et al., 1999).

5. Summary

(1) We have obtained high precision creep data for melt-free, dry Fo–En composites. The creep behavior of the Fo–En composites can be described by a power-law flow law with $n = 1.3–2.0$ and $Q = 472–584$ kJ/mol. The measured n and Q values increase with decreasing V_{Fo}. The mechanical data and TEM microstructural observations suggest that the En deformed mainly by dislocation creep while the Fo deformed by dislocation-accommodated diffusion creep under the experimental conditions. No change has been observed in deformation mechanism of each phase when in the composites, compared to when it is in a single-phase aggregate.

(2) The pure Fo aggregate is stronger than the pure En aggregate, and the flow strength contrast between these phases is about 3–8, depending on the experimental conditions. The bulk strength of the Fo–En composites increases non-linearly with V_{Fo} and a dramatic increase in the flow strength occurs at $V_{Fo} = 0.4–0.6$, which is interpreted as resulting from the transition from a weak-phase supported (WPS, $V_{Fo} < 0.4$) to a strong-phase supported (SPS, $V_{Fo} > 0.6$) structures.

(3) The Fo–En composite rheological data have been compared with various theoretical models to evaluate their applicability. The comparisons indicate that none of the existing models can give a precise predication if the model is applied to the entire V_{Fo} range from 0 to 1. WPS-based models such as Takeda (1998) mode 2, Ji and Zhao (1993) lower bound, the shear-lag model, Zhao–Ji WPS model, and Yoon–Chen model yield a good prediction for the flow strength of En–Fo composites within the range of $V_{Fo} < 0.4$. SPS-based models such as Zhao–Ji SPS model, Ji–Zhao upper bound, and Tharp model are good for composites with $V_{Fo} > 0.60$. In the transitional regime ($V_{Fo} = 0.40–0.60$), however, none of these models have taken into consideration the phase-interpenetrating structure of the composites and thus none give a good estimate for the composite flow strength. Applications of the WPS- and SPS-based models into the transitional regime result in under- and over-estimations for the composite flow strength, respectively. There is thus a need to develop theoretical models suitable for the transitional regime; these models are important for modeling the rheological behavior and tectonic deformation of the Earth's crust and upper mantle which are polyphase composites.

Acknowledgements

We thank the NSERC of Canada for research grants. Ji would like to thank the Alexandre von Homboldt Stiftung for a visiting fellowship. This fellowship allowed him to pass his sabbatical year in Prof. Georg Dresen's laboratory (GFZ-Potsdam, Germany). We are grateful to J. Tullis, K.V. Hodges and an anonymous reviewer for their thoughtful reviews of the manuscript. This is LITHOPROBE contribution No. 1222.

References

Anastasiou, P., Seifert, F., 1972. Solid solubility of Al_2O_3 in enstatite at high temperatures and 1-5 kb water pressure. Contrib. Mineral. Petrol. 34, 272–287.

Arzi, A.A., 1978. Critical phenomena in the rheology of partially melted rocks. Tectonophysics 44, 173–184.

Bai, Q., Mackwell, S.J., Kohlstedt, D.L., 1991. High-temperature creep of olivine single crystals: 1. Mechanical results for buffered samples. J. Geophys. Res. 96, 2441–2463.

Bao, G., Hutchinson, J.W., McMeeking, R.M., 1991. Particle reinforcement of ductile matrices against plastic flow and creep. Acta Metall. Mater. 39, 1871–1882.

Bass, J.D., 1995. Elasticity of minerals, glasses, and melts. In: Ahrens, T.J. (Ed.), Mineral Physics and Crystallography: A Handbook of Physical Constants. American Geophysical Union, Washington, DC, pp. 45–63.

Bloomfield, J.P., Covey-Crump, J., 1993. Correlating mechanical data with microstructural observations in deformation experiments on synthetic two-phase aggregates. J. Struct. Geol. 15, 1007–1019.

Bruhn, D.F., Olgaard, D.L., Dell'Angelo, L.N., 1999. Evidence for enhanced deformation in two-phase rocks: experiments on the rheology of calcite–anhydrite aggregates. J. Geophys. Res. 104, 707–724.

Burg, J.P., Wilson, C.J.L., 1987. Deformation of two phase systems with contrasting rheology. Tectonophysics 135, 199–205.

Chakraborty, S., Farver, J.R., Yund, R.A., Rubie, D.C., 1992. Mg tracer diffusion in forsterite and San Carlos olivine. EOS Trans. AGU 73, 373.

Chopra, P.N., 1986. The plasticity of some fine-grained aggregates of olivine at high pressure and temperature. In: Hobbs, B.E., Heard, H.C. (Eds.), Mineral and Rock Deformation: Laboratory Studies. American Geophysical Union, Washington, DC, pp. 25–34.

Clarke, D.R., 1992. Interpenetrating phase composites. J. Am. Ceram. Soc. 75, 739–759.

Cox, H.L., 1952. The elasticity and strength of paper and other fibrous materials. Br. J. Appl. Phys. 3, 72–79.

Daines, M.J., Kohlstedt, D.L., 1996. Rheology of olivine–pyroxene aggregate. EOS Trans. AGU 77, 711.

Darot, M., Gueguen, Y., 1981. High-temperature creep of forsterite single crystals. J. Geophys. Res. 86, 6219–6234.

Dell'Angelo, L.N., Tullis, J., 1996. Textural and mechanical evolution with progressive strain in experimentally deformed aplite. Tectonophysics 256, 57–82.

Dresen, G., Evans, B., Olgaard, D.L., 1998. Effect of quartz inclusions on plastic flow in marble. J. Geophys. Lett. 25, 1245–1248.

Drury, M.R., Fitz Gerald, J.D., 1996. Grain boundary melt films in an experimentally deformed olivine–orthopyroxene rocks: implications for melt distribution in upper mantle rocks. Geophys. Res. Lett. 23, 701–704.

Duva, J.M., 1984. A self-consistent analysis of the stiffening effect of rigid inclusions on a power-law material. J. Eng. Mater. Technol. 106, 317–321.

Fliervoet, T.F., Drury, M.R., Chopra, P.N., 1999. Crystallographic preferred orientations and misorientations in some olivine rocks

deformed by diffusion or dislocation creep. Tectonophysics 303, 1–27.

Gilotti, J.A., 1992. The rheological critical matrix in arkosic mylonites along the Särv Thrust, Swedish Caledonides. In: Mitra, S., Fisher, G.W. (Eds.), Structural Geology of Fold and Thrust Belts. Johns Hopkins Univ. Press, Baltimore, pp. 145–160.

Griffiths, T.J., Davies, R., Bassett, M.B., 1979. Analytical study of effects of pore geometry on tensile strength of porous materials. Power Metall. 22, 119–123.

Gurland, J., 1979. A structural approach to the yield strength of two-phase alloys with coarse microstructures. Mater. Sci. Eng. 40, 59–71.

Handy, M.R., 1994. Flow laws for rocks containing two non-linear viscous phases: a phenomenological approach. J. Struct. Geol. 16, 287–301 (also see his Correction, J. Struct. Geol. 16, 1727, 1994).

Hirth, G., Kohlstedt, D.L., 1995. Experimental constraints on the dynamics of the partially molten upper mantle: deformation in diffusion creep regime. J. Geophys. Res. 100, 1981–2001.

Hitchings, R.S., Paterson, M.S., Bitmead, J., 1989. Effect of iron and magnetite additions in olivine–pyroxene rheology. Phys. Earth Planet. Inter. 55, 277–291.

Hull, D., Clyne, T.W., 1996. An introduction to Composite Materials. Cambridge University Press, New York.

Jaoul, O., Froidevaux, C., Durham, W.B., Michaut, M., 1980. Oxygen self-diffusion in forsterite: implications for the high-temperature creep mechanism. Earth Planet. Sci. Lett. 47, 391–397.

Jaoul, O., Poumellec, M., Froidevaux, C., Havette, C., 1981. Silicon diffusion in forsterite: a new constraint for understanding mantle deformation. In: Stacey, F.D., Paterson, M.S., Nicolas, A. (Eds.), Anelasticity in the Earth. Am. Geophys. Union, Washington, DC, pp. 95–100.

Ji, S., Wang, Z.C., 1999. Elastic properties of forsterite–enstatite composites up to 3.0 GPa. J. Geodyn. 28, 147–174.

Ji, S., Zhao, P., 1993. Flow laws of multiphase rocks calculated from experimental data on the constituent phases. Earth Planet. Sci. Lett. 117, 181–187.

Ji, S., Zhao, P., 1994. Strength of two-phase rocks: a model based on fiber-loading theory. J. Struct. Geol. 16, 253–262.

Ji, S., Zhu, Z.M., Wang, Z.C., 1998. Relationship between joint spacing and bed thickness in sedimentary rocks in the Saint-Jean-Port-Joli area of Quebec Appalachians: effects of interbed slip. Geol. Mag. 135, 637–655.

Ji, S., Jiang, Z., Wirth, R., 1999. Crystallographic preferred orientation (CPO) of experimentally sheared plagioclase aggregates: implications for crustal heterogeneity (abstract). EOS Trans. AGU 80, 916.

Ji, S., Wirth, R., Rybacki, E., Jiang, Z., 2000. High-temperature plastic deformation of quartz-plagioclase multilayers by layer-normal compression. J. Geophys. Res. 105, 16651–16664.

Jordan, P., 1987. The deformational behavior of bimineralic limestone–halite aggregates. Tectonophysics 135, 185–197.

Jordan, P., 1988. The rheology of polymineralic rocks—an approach. Geol. Rundsch. 77, 285–294.

Karato, S., Paterson, M.S., Fitz Gerald, J.D., 1986. Rheology of synthetic olivine aggregates: influence of grain size and water. J. Geophys. Res. 91, 8151–8176.

Kelly, A., Macmillan, N.H., 1986. Strong Solids Oxford Science Publications, Oxford.

Kelly, A., Street, K.N., 1972. Creep of discontinuous fiber composites: II. Theory for the steady-state. Proc. R. Soc. London, Ser. A 328, 283–293.

Kirby, S.H., Christie, J.M., 1977. Mechanical twinning in diopside $Ca(Mg,Fe)Si_2O_6$: structural mechanism and associated crystal defects. Phys. Chem. Miner. 1, 137–163.

Kohlstedt, D.L., Evans, B., Mackwell, S.J., 1995. Strength of the lithosphere: constraints imposed by laboratory experiments. J. Geophys. Res. 100, 17587–17602.

Kohlstedt, D.L., Bai, Q., Wang, Z.C., Mei, S., 2000. Rheology of partially molten rocks. In: Bagdassarov, N., LaPorte, D., Thompson, A.B. (Eds.), Physics and Chemistry of Partially Molten Rocks, Kluwer Academic Publishing, Boston, pp. 3–28.

Kronenberg, A.K., Shelton, G.L., 1980. Deformation microstructures in experimentally deformed Maryland diabase. J. Struct. Geol. 2, 341–353.

Lange, F.F., Davis, B.I., Clarke, D.R., 1980. Compressive creep of Si_3N_4/MgO alloys: Part 1. Effect of composition. J. Mater. Sci. 15, 601–610.

Lawlis, J., 1997. Experimental deformation of olivine–enstatite aggregates. Unpublished PhD thesis, Pennsylvania State University.

Li, P., Wang, Z.C., Karato, S., 1996. High-temperature creep in fined-grained polycrystalline $CaTiO_3$, an analogue material of $(Mg,Fe)SiO_3$ perovskite. Phys. Earth Planet. Inter. 95, 19–36.

Mackwell, S., Kohlstedt, D.L., 1986. High-temperature deformation of forsterite single crystals doped with vanadium. Phys. Chem. Miner. 13, 351–356.

Mackwell, S.J., Zimmerman, M.E., Kohlstedt, D.L., 1998. High-temperature deformation of dry diabase with application to tectonics on Venus. J. Geophys. Res. 103, 975–984.

McDonnell, R.D., Peach, C.J., van Roermund, H.L.M., Spiers, C.J., 2000. Effect of varying enstatite content on the deformation behavior of fine-grained synthetic peridotite under wet conditions. J. Geophys. Res. 105, 13535–13553.

Nardone, V.C., Prewo, K.M., 1986. On the strength of discontinuous silicon carbide reinforced aluminum composites. Scr. Metall. 20, 43–48.

Paterson, M.S., 1989. The interaction of water with quartz and its influence in dislocation flow—an overview. In: Karato, S., Torium, M. (Eds.), Rheology of Solids and of the Earth. Oxford Science Publications, New York, pp. 107–142.

Poirier, J.P., 1985. Creep of Crystals. Cambridge Univ. Press, New York.

Presnall, D.C., 1995. Phase diagrams of Earth-forming minerals. In: Ahrens, T.J. (Ed.), Mineral Physics and Crystallography, A Handbook of Physical Constants. America Geophysical Union, Washington, pp. 248–267.

Raj, R., 1982. Separation of cavitation-strain and creep strain during deformation. J. Am. Ceram. Soc. 65, 46–48.

Raleigh, C.B., Kirby, S.H., Carter, N.L., Ave Lallemant, H.G., 1971. Slip and the clinoenstatite transformation as competing processes in enstatite. J. Geophys. Res. 76, 4011–4022.

Ravichandran, K.S., Seetharaman, V., 1993. Prediction of steady state creep behavior of two-phase composites. Acta Metall. Mater. 41, 3351–3361.

Relandeau, C., 1981. High temperature creep of forsterite polycrystalline aggregates. Geophys. Res. Lett. 8, 733–736.

Ricoult, D.L., Kohlstedt, D.L., 1985. Experimental evidence for the effect of chemical environment upon the creep rate of olivine. In: Shock, R.N. (Ed.), Point Defects in Minerals. Geophys. Monogr. Ser., vol. 31. AGU, Washington, DC, pp. 171–184.

Ross, J.V., Nielsen, K.C., 1978. High-temperature flow of wet polycrystalline enstatite. Tectonophysics 44, 233–261.

Ross, J.V., Bauer, S.J., Hansen, F.D., 1987. Texture evolution of synthetic anhydrite–halite mylonite. Tectonophysics 140, 307–326.

Rutter, E.H., Neumann, D.H.K., 1995. Experimental deformation of partially molten Westerly granite under fluid-absent conditions, with implications for the extraction of granitic magma. J. Geophy. Res. 100, 15697–15715.

Takeda, Y.T., 1998. Flow in rocks modeled as multiphase continua: application to polymineralic rocks. J. Struct. Geol. 20, 1569–1578.

Tharp, T.M., 1983. Analogies between the high-temperature deformation of polyphase rocks and the mechanical behavior of porous powder metal. Tectonophysics 96, T1–T11.

Tsai, R.L., Raj, R., 1982. Overview 18: creep fracture in ceramics containing small amount of a liquid phase. Acta Metall. 30, 1043–1058.

Tullis, J., Wenk, H.R., 1994. Effect of muscovite on the strength and lattice preferred orientations of experimentally deformed quartz aggregates. Mater. Sci. Eng. A 175, 209–220.

Tullis, T.E., Horowitz, F.G., Tullis, J., 1991. Flow law of polyphase aggregates from end-member flow laws. J. Geophys. Res. 96, 8081–8096.

Unskov, E.P., 1961. An Engineering Theory of Plasticity. Butterworths, London.

Wheeler, J., 1992. Importance of pressure solution and Coble creep in the deformation of polymineralic rocks. J. Geophys. Res. 97, 4586–4597.

Wirth, R., 1996. Thin amorphous films (1–2 nm) at olivine grain boundaries in mantle xenoliths from San Carlos, Arizona. Contrib. Mineral. Petrol. 124, 44–54.

Xiao, X., 1999. Experimental Study of the Rheology of Synthetic Anorthite-Quartz Aggregates. GeoForschungsZentrum Potsdam, Germany, Scientific Technical Report STR99/14, 125 pp.

Yoon, C.K., Chen, I.W., 1990. Superplastic flow of two-phase ceramics containing rigid inclusions-zirconia/mullite composites. J. Am. Ceram. Soc. 73, 1555–1565.

Zhao, P., Ji, S., 1994. Creep analysis of two-phase rocks. Canadian Lithoprobe Abitibi-Grenville Project Report 41, pp. 159–164.

Zhao, P., Ji, S., 1997. Refinements of shear-lag model and its applications. Tectonophysics 279, 37–53.